Projected effects of climate change on *Pseudo-nitzschia* bloom dynamics in the Gulf of Maine

Suzanna Clark [1,2], Katherine A. Hubbard [3], Dennis J. McGillicuddy, Jr.[4], David K. Ralston[4], Michael A. Alexander[5], Enrique Curchitser[6], Charles Stock[7]*

[1] MIT/WHOI Joint Program in Oceanography/Applied Ocean Sciences and Engineering
86 Water St. Woods Hole, MA, 02543, USA
[2] University of Minnesota
Minneapolis, MN 55455
* Corresponding author: sclark@whoi.edu
[3] Florida Fish and Wildlife Conservation Commission-Fish and Wildlife Research Institute,
100 8th Ave SE, St. Petersburg, FL, 33701, USA
[4] Woods Hole Oceanographic Institution
86 Water St. Woods Hole, MA, 02543, USA
[5] NOAA/Physical Sciences Laboratory
325 Broadway, Boulder, CO 80305
[6] Rutgers University
57 US Highway 1. New Brunswick, NJ 08901-8554
[7] NOAA Geophysical Fluid Dynamics Laboratory
201 Forrestal Road, Princeton, NJ 08540-6649

Abstract

Worldwide, warming ocean temperatures have contributed to extreme harmful algal bloom events and shifts in phytoplankton species composition. In 2016 in the Gulf of Maine (GOM), an unprecedented *Pseudo-nitzschia* bloom led to the first domoic-acid induced shellfishery closures in the region. Potential links between climate change, warming temperatures, and the GOM *Pseudo-nitzschia* assemblage, however, remain unexplored. In this study, a global climate change projection previously downscaled to 7-km resolution for the Northwest Atlantic was further refined with a 1–3-km resolution simulation of the GOM to investigate the effects of climate change on HAB dynamics. A 25-year time slice of projected conditions at the end of the 21st century (2073–2097) was compared to a 25-year hindcast of contemporary ocean conditions (1994–2018) and analyzed for changes to GOM inflows, transport, and *Pseudo-nitzschia australis* growth potential. On average, climate change is predicted to lead to increased temperatures, decreased salinity, and increased stratification in the GOM, with the largest changes occurring in the late summer. Inflows from the Scotian Shelf are projected to increase, and alongshore transport in the Eastern Maine Coastal Current is projected to intensify. Increasing ocean temperatures will likely make *P. australis* growth conditions less favorable in the southern and western GOM but improve *P. australis* growth conditions in the eastern GOM, including a later growing season in the fall, and a longer growing season in the spring. Combined, these changes suggest that *P. australis* blooms in the eastern GOM could intensify in the 21st century, and that the overall *Pseudo-nitzschia* species assemblage might shift to warmer-adapted species such as *P. plurisecta* or other *Pseudo-nitzschia* species that may be introduced.

1 Introduction

Pseudo-nitzschia is a lightly silicified, pennate diatom genus with at least 52 confirmed species (Bates et al., 2018). Twenty-six species have been confirmed to produce domoic acid (DA), a neurotoxin that can cause amnesic shellfish poisoning. *Pseudo-nitzschia* has been described as a "cosmopolitan" genus (Hasle, 2002), because species exist across a wide range of temperature and salinity conditions and have been observed globally (Bates et al., 2018). The severity and range of harmful algal blooms (HABs) caused by *Pseudo-nitzschia* have both been increasing in recent years, with large-scale blooms leading to millions of dollars in economic losses (Moore et al., 2020), and species blooming in previously unaffected regions (e.g. Bates et al., 2018; Clark et al., 2019; Park et al., 2018).

One example of the increasing abundance and extent of *Pseudo-nitzschia* HABs is an unprecedented DA event and subsequent shellfishery closures in the Gulf of Maine (GOM) in 2016 (Bates et al., 2018; Clark et al., 2019). Prior to 2016, 14 *Pseudo-nitzschia* species had been identified in the region (Fernandes et al., 2014), including some DA producers, but the 2016 bloom was caused primarily by *P. australis*, which had never before been observed in the GOM (Clark et al., 2019). *P. australis* blooms have occurred every year since 2016, reflecting a possible regime shift in *Pseudo-nitzschia* bloom dynamics (Clark et al., 2021).

The DA event in 2016 is but one example of recent changes in the GOM. Although the rate of warming in the GOM and its effect on ecosystems is under debate (Palmer et al., 2016; Pershing et al., 2016, 2015), there is no question that sea surface temperatures are warming, and that the warming is strongest in the summer and autumn (Thomas et al., 2017a), the time of year when previous toxic *Pseudo-nitzschia* blooms – including *P. australis* – have occurred. Two marine heat waves have been observed in the region in recent years, one in 2012 and one in 2016 (Pershing et al., 2018, 2015). In addition, the relative importance of different source waters to the GOM may have changed in recent decades: Townsend et al. (2015) provided evidence that the proportion of Scotian Shelf Water flowing into the region has increased relative to Slope Water. Meanwhile, a northward shift in the Gulf Stream may favor inflows of warm slope water along the Gulf of Maine shelf break, and this pattern may strengthen over the 21st century (Saba et al.,

2016). Such changes to the inflows to the GOM could affect water mass properties in the interior, and potentially future growth conditions for GOM HABs like *Pseudo-nitzschia*.

Changes to the environmental conditions in the GOM and its source waters might affect the existing assemblage of *Pseudo-nitzschia*. Studies in other regions have shown that increasing temperatures might increase *Pseudo-nitzschia* growth rates (Thorel et al., 2014), or favor *Pseudo-nitzschia* over other phytoplankton (Zhu et al., 2017). Higher temperatures can also increase DA production, particularly in *P. australis* (McKibben et al., 2017; Thorel et al., 2014; Zhu et al., 2017). Indeed, some changes to *Pseudo-nitzschia* abundance worldwide have already occurred as a result of warming oceans. One illustration is the record-breaking *P. australis* bloom on the U.S. West Coast in 2015 that coincided with the North Pacific Ocean Warm Anomaly and peaked during intermittent upwelling of water with a low silica-to-nitrate ratio (McCabe et al., 2016; Ryan et al., 2017). The response of *P. australis* to climate change in other regions may depend on the environment and *P. australis* population in question (Trainer et al., 2020). Warming ocean temperatures over the 20th Century were correlated with an increase in *Pseudo-nitzschia* species and *P. australis* specifically in the Santa Barbara Basin, (Barron et al., 2013), while increased temperatures along with increased nitrogen loading in Danish sill-fjords may have contributed to a shift in the *Pseudo-nitzschia* species assemblages on decadal time scales (Lundholm et al., 2010).

In the context of these global changes, the appearance of *P. australis* in the GOM in 2016, and annual toxic *P. australis* blooms in the GOM since 2016, it is important to project how *Pseudo-nitzschia* blooms in the GOM might vary in the future. Clark et al. (2021) outlined how *P. australis* blooms could be a growing concern in the region through persistent introduction, despite insufficient evidence to indicate a regime shift in 2016. Models offer an ideal tool for projections, but a typical Global Climate Model is too coarsely resolved (about 1-degree resolution) to represent the nearshore processes and complex bathymetry that are important to hydrodynamics and HAB dynamics in the GOM. For example, a 1-degree model cannot resolve the Gulf of Maine Coastal Current, which transports HABs from the eastern GOM to the western GOM (Keafer et al., 2005; Li et al., 2009). Coarser models also do not capture slope water inflows through the Northeast Channel (Shin and Alexander, 2020a), which are important for the interior

water properties of the GOM and for introducing HAB species to the region (Clark et al., 2021; Hebert et al., 2018).

One solution is to downscale a coarse circulation model to a GOM regional model (Drenkard et al., 2021; Ralston and Moore, 2020). This approach was used to model the Northwest Atlantic from the Gulf of Mexico to the Gulf of St. Lawrence at a 7-km horizontal resolution (Alexander et al., 2020). The higher resolution model predicted enhanced bottom warming in the GOM relative to the climate models, because its finer resolution better captured ocean circulation, deep inflows in the Northeast Channel, and altered upstream water mass properties (Shin and Alexander, 2020a).

This study will further downscale the 7-km-resolution model (Alexander et al., 2020) to a 1–3-km resolution GOM Regional Ocean Modeling System (ROMS) (He et al., 2008; Li et al., 2009; McGillicuddy et al., 2011) to investigate the effects of climate change on *Pseudo-nitzschia* bloom dynamics in the GOM. The high-resolution GOM ROMS has been shown to capture alongshore transport and hydrographic variability between sub-regions of the Gulf of Maine that are important to regional HAB dynamics (Clark et al., 2021; He et al., 2008; Li et al., 2020, 2015, 2009; McGillicuddy et al., 2011; McGillicuddy et al., 2014). To our knowledge, this is the first study to investigate the effects of climate change on *Pseudo-nitzschia* with a physical circulation model. The following methods section describes the study region, the two ROMS configurations, the downscaling approach, and associated analyses. The results and discussion section will focus on changes to temperature and hydrodynamics, the mechanics thereof, and their consequences for *Pseudo-nitzschia* blooms. Particular attention is given to how *P. australis* bloom dynamics might change in the eastern GOM, a region that has seen shellfishery closures due to DA toxicity nearly every year since 2016.

2 Methods

2.1 Region of Study

2.1.1 Gulf of Maine

The Gulf of Maine is a shelf sea off the coast of the northeast United States and Canada, between 42 and 44.5°N and 66 and 71°W (Figure 1). Mean sea surface temperatures (SST) range from 4°C

in February to 22.5℃ in August, and historical salinity values generally range from 29 to 33.5 PSU (Li et al., 2014). Interior water mass properties are largely driven by inflows, which enter the gulf along the coast south of Nova Scotia and at depth in the Northeast Channel (Townsend et al., 2015). Nova Scotian inflows comprise relatively fresh, cool Scotian Shelf Water (5–7℃, 32.5–33.4 PSU), while Northeast Channel inflows are a mixture of Warm Slope Water (11℃, 35 PSU), and Labrador Slope Water (6.5℃, 34.5 PSU) (Townsend et al., 2015, 2014). Portions of the Bay of Fundy, Georges Bank, and northeastern GOM are well-mixed year-round because of the energy imparted by the tides (Townsend et al., 2014). The Gulf of Maine is warming rapidly, at a rate of approximately 0.4℃ decade^{-1} (Chen et al., 2020; Pershing et al., 2015).

The interior GOM is comprised of three basins with depths greater than 200m – Georges Basin, Wilkinson Basin, and Jordan Basin – and is separated from the open North Atlantic via offshore banks shallower than 100m – Georges Bank and Browns Bank. The general circulation in the GOM is cyclonic, with anticyclonic circulation around Georges Bank (Bigelow, 1927; Brooks, 1994; Xue et al., 2000). Alongshore flow on the coast of Maine is divided into the buoyancy-driven Maine Coastal Current, and the GOM Coastal Plume (Bisagni et al., 1996; Keafer et al., 2005; Pettigrew et al., 2005), which is fed by the region's five largest rivers, the St. John, Penobscot, Merrimack, Kennebec, and Androscoggin.

2.2 Scotian Shelf

Upstream of the GOM is the Scotian Shelf, a shelf sea that stretches from 42.5 to 45.5°N and from 57 to 65.5°W. The 30-year (1981–2010) climatological annual mean SST ranges from 7.1℃ on the Eastern Scotian Shelf to 8.1℃ on the Western Scotian Shelf, and water temperatures have been warming at an average rate of 0.5℃ decade^{-1} (Hebert et al., 2018). The Scotian Shelf is relatively shallow, with depths ranging from 0–200m and several banks shallower than 100m (Hebert et al., 2018). The two main currents, the Nova Scotia Current and the Labrador Current, both flow from the northeast to the southwest, with the Nova Scotia Current along the coast and the Labrador Current along the shelf break (Townsend et al., 2006). The main upstream sources of Scotian Shelf water are the Gulf of St. Lawrence and the Labrador Current.

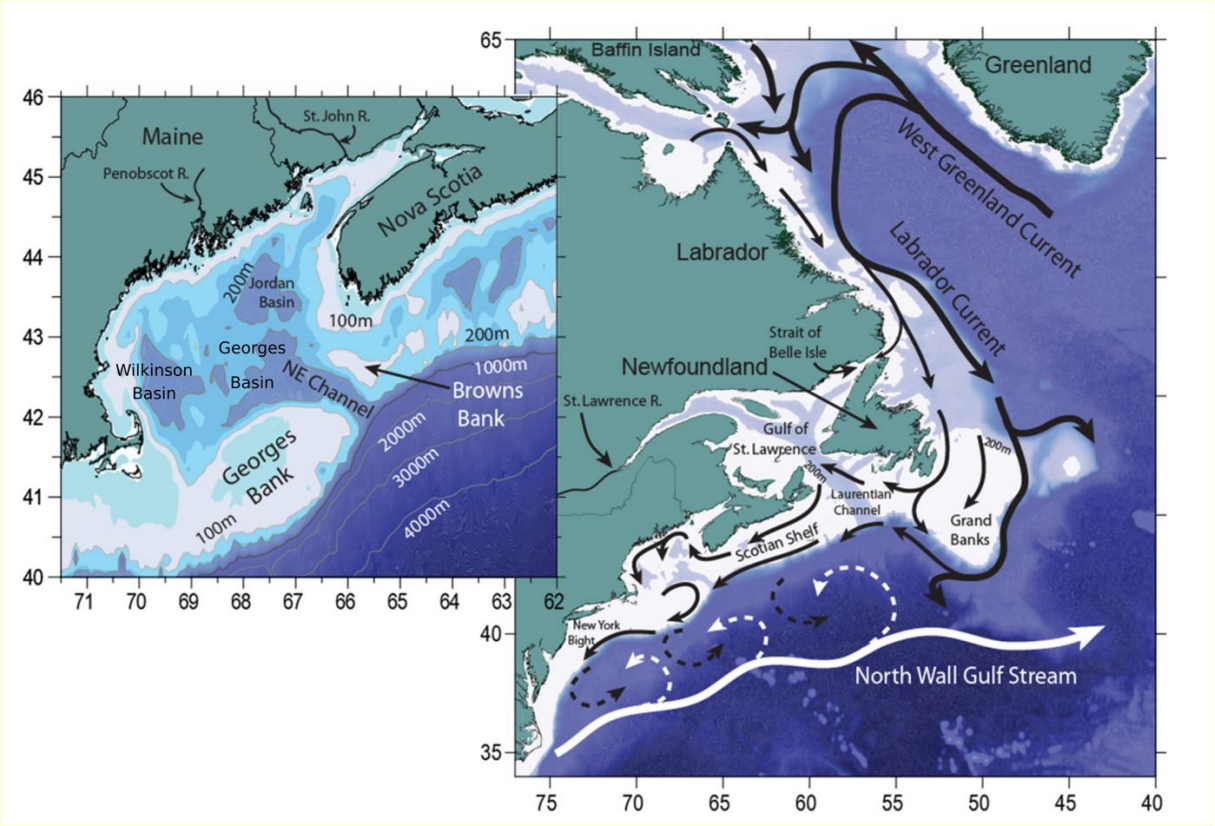

Figure 1. From Townsend et al. (2010)[8]: "Map of the NW Atlantic Ocean, Labrador Sea and Gulf of Maine, showing the major current systems (after Chapman and Beardsley, 1989; Loder et al., 1998) … Dashed arrows indicate mixing of waters (not currents) in the slope sea (Csanady and Hamilton, 1988). Inset shows location of the Northeast Channel (sill depth ca. 220 m) and the channel between Browns Bank and Nova Scotia (depth ca. 150 m)."

2.3 Models

A series of one-way nested models were used to simulate the impact of climate change on the hydrographic and circulation patterns within the Gulf of Maine that are linked to HAB dynamics: the Geophysical Fluid Dynamics Laboratory's Earth System Model (GFDL-ESM2M), the Northwest Atlantic ROMS, and the Gulf of Maine ROMS.

2.3.1 Climate Model

The global earth system model GFDL-ESM2M (Dunne et al., 2013, 2012) was used to force the Northwest Atlantic ROMS in Alexander et al. (2020). Atmospheric resolution in the GFDL-ESM2M

[8]This figure was published in Continental Shelf Research, Vol 30; Townsend, David W., Rebuck, Nathan D., Thomas, Maura A., Karp-Boss, Lee, Gettings, Rachel M., "A changing nutrient regime in the Gulf of Maine", p. 820–832, Copyright Elsevier (2010).

is 2°(lat) x 2.5°(lon) with 24 vertical levels, and the oceanographic resolution is approximately 1° x 1°, with 50 vertical levels (Dunne et al., 2012). The climate simulations that were used in Alexander et al. (2020) were projected with the RCP8.5 emissions pathway, the highest Representative Concentration Pathway defined by the Intergovernmental Panel for Climate Change (IPCC) (IPCC, 2014). Under this scenario, radiative forcing exceeds 8.5 W m^{-2} by 2100. Refer to Dunne et al. (2012, 2013) for more details about the GFDL-ESM2M configuration and Alexander et al. (2020) for comparisons of North Atlantic projections between GFDL-ESM2M and other climate models. The potential effects of climate model selection and differences between climate model projections are discussed more in Section 4.

2.3.2 Regional Ocean Modeling System

The Regional Ocean Modeling System (ROMS) is a hydrostatic, free surface, split-explicit, terrain-following primitive equation model (Shchepetkin and McWilliams, 2003, 2005). Two different configurations are relevant to this study, the Northwest Atlantic ROMS and the GOM ROMS.

2.3.2.1 Northwest Atlantic ROMS

The Northwest Atlantic ROMS (NWA ROMS) covers the shelf sea and part of the open ocean along the east coast of North America from the Gulf of Mexico to the Gulf of St. Lawrence, between 10°N and 50°N (Kang and Curchitser, 2013) (Figure 2). Its horizontal resolution is 7 km and it has 40 vertical layers, with higher resolution near the surface. The boundary and initial conditions for the historical run were extracted from the Simple Ocean Data Assimilation (SODA v2.1.6) (Carton and Giese, 2008), which has 0.5° horizontal resolution and 40 vertical layers. Historical surface forcing was taken from the Coordinated Ocean-Ice Reference Experiments (CORE v2), which has a 6-hour temporal resolution and 1.9° spatial resolution (Large and Yeager, 2009). Historical river discharge from the continental discharge database (Dai et al., 2009) was used to implement freshwater fluxes directly into the model's surface grid cells. Results from the control simulation (1976–2005) and the projection (2070–2099) were saved as 5-day averages. The reader is referred to Kang and Curchitser (2013) for more details about the model setup and to Alexander et al. (2020) for specifics about the climate simulations.

2.3.2.2 Gulf of Maine ROMS

The Gulf of Maine ROMS (GOM ROMS) includes the GOM from Georges Bank in the South to the Bay of Fundy in the North (38.7°N to 46.6°N), and from Coastal New England in the West to the Scotian Shelf in the East (72.9°W to 62.0°W) (Figure 2). The horizontal resolution ranges from 1 to 3 km, and there are 36 vertical terrain-following layers.

The contemporary ocean simulation is based on the system described in He and McGillicuddy (2008), Li et al. (2009), and McGillicuddy et al. (2011). Boundary conditions for temperature, salinity, velocity, and sea surface height for the GOM ROMS were extracted from HYCOM (Hybrid Coordinate Ocean Model) experiment GOFS3.0, which was interpolated to the GOM ROMS grid. HYCOM has a 1/12° resolution in the horizontal and 40 layers in the vertical, and simulations from GOFS3.0 are available from 1994–2018 at 3-day intervals. HYCOM utilizes hybrid vertical coordinates, with isopycnal vertical layers in the open stratified ocean, terrain-following sigma layers in the coastal ocean, and z-coordinates in unstratified areas. Atmospheric forcing in the GOM ROMS was specified via bulk formulation with data from the North American Regional Reanalysis (NARR), which has 6-hour temporal resolution and 1/6° spatial resolution (Mesinger et al., 2006). The five largest rivers in the GOM (St. John, Penobscot, Kennebec, Androscoggin, and Merrimack) are included in the GOM ROMS forcing files as daily volume transport ($m^3\ s^{-1}$) as measured by U.S. Geological Survey river gauges (USGS, 2013). A volumetric adjustment was added to each river to account for drainage area downstream of the gauge. Multi-scale Ultra-High-Resolution Temperature (MUR4.1) from satellites was used for a surface heat flux correction (Chin et al., 2017).

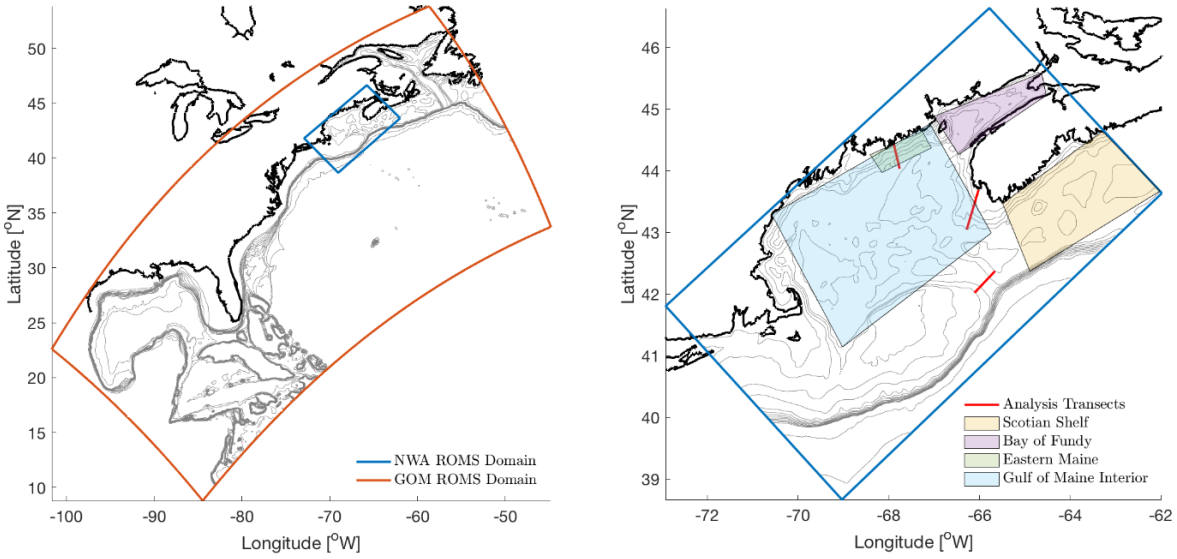

Figure 2. (left) The Northwest Atlantic (NWA) ROMS Domain (red outline) and Gulf of Maine (GOM) ROMS Domain (blue outline). Bathymetry is drawn every 100m from 0 to 1000m, at 2000m, and at 3000m according to the bathymetry of the NWA ROMS. The bold black line indicates the coastline. (right) The GOM ROMS domain (blue outline) with transect locations indicated with red lines and important sub-regions indicated with shaded boxes. Bathymetry is drawn every 25m from the surface to 100m, every 100m to 1000m, and at 2000m and 3000m. The bold black line indicates the coastline.

2.4 Experimental Setup

The GOM ROMS was run for 25 consecutive years as a hindcast (1994–2018) and projection (2073–2097). Boundary and initial conditions for the hindcast runs were created from the sources detailed in Section 2.3.2, while the climate change runs were forced with the Delta Method, detailed below.

2.4.1 Delta Method

The NWA ROMS climate projections were downscaled to the GOM ROMS region via the Delta Method, as described in Alexander et al. (2020) and Shin and Alexander (2020). This method calculates the long-term (i.e. multi-decadal) mean difference in oceanic and atmospheric conditions between the projected and contemporary climate states in a lower resolution model (in this case, the NWA ROMS) and adds this difference (i.e. the Delta) to the initial and boundary conditions of a higher resolution model (the GOM ROMS). Here the Deltas were calculated monthly, because climate change impacts are likely to have seasonal variation (Shin and Alexander, 2020). Because the same Deltas are added to each hindcast year to create the projection, this method does not account for potential changes in forcing variability as a result of

climate change. Rather, forcing variability in the contemporary ocean is preserved, but seasonal means have been shifted in a manner consistent with climate change projections. The sources from which Deltas were calculated and the fields to which they were added are detailed in the Supplementary Material in Table S-3.

The Delta Method was implemented as follows:

1. A 30-year monthly mean for each forcing field at the beginning and the end of the 21st Century was calculated from the sources in Table S-3. Atmospheric Deltas were calculated from the NWA ROMS forcing files, which were created from the GFDL-ESM2M climate simulations.
2. Twelve Deltas (one for each month) were calculated by subtracting the hindcast means from the climate simulation means.
3. The hindcast time periods for the NWA ROMS (1976–2005) and the GOM ROMS (1994–2018) were not the same because of the availability of the HYCOM simulations used to provide boundary conditions for the GOM ROMS. As a result – using 2084 as the mid-point of the projection time period – the average time difference between projection and hindcast in the NWA ROMS simulations was 94 years (2084–1990), while the average difference between the projection and hindcast in the GOM ROMS simulations was 78 years (2084–2006). Deltas were multiplied by 78/94 to account for the difference, creating a "Fractional Delta". This assumes that the Deltas increase linearly with time, which is a simplifying assumption.
4. Fractional Deltas were spatially and temporally interpolated to the required resolution for the GOM ROMS initial and boundary conditions. In this study, this meant that oceanographic Deltas were interpolated to the HYCOM grid, atmospheric Deltas were interpolated to the NARR grid, and SST Deltas were interpolated to the satellite grid.
5. Interpolated fractional Deltas were added to the appropriate forcing files for the GOM ROMS climate simulations.
6. The GOM ROMS was run consecutively for 25 years (representing 2073–2097) with the new forcing files.

River inputs are implemented differently in the NWA ROMS and GOM ROMS configurations, so the river Deltas were relative: the monthly average percent change between hindcast and projection in the river inputs was calculated from the NWA ROMS input files, and that percent change was applied to the river discharge in the GOM ROMS input files.

2.5 Analysis

2.5.1 Hydrodynamic Analyses

Three transects were chosen for transport analysis: across the Northeast Channel (42.02°N, 66.11°W to 42.37°N, 65.66°W), perpendicular to Nova Scotia (42.62°N, 66.57°W to 43.69°N, 66.02°W), and cross-shore from Mt. Desert Island across the Eastern Maine Coastal Current (EMCC) (44.43°N, 67.89°W to 44.03°N, 67.76°W) (Figure 2). At each transect, velocities were projected in the alongshore direction (along-channel in the Northeast Channel) according to the angle of the coastline (channel) with respect to east (Figure 2) such that positive velocities were toward the GOM. At the EMCC, positive velocities were toward the southwest, the predominant flow direction. Transport toward the GOM was calculated by multiplying the projected velocity in each grid cell where $u > 0$ by the cell's cross-sectional area and summing over the transect. Transport *toward* the GOM was used, rather than *net* transport, because the analysis focused on the ability to carry cells into the GOM. In addition, transport into the GOM in the Northeast Channel is of a similar magnitude as transport out due to strongly sheared flow, and thus the net transport obscures the inflow signal. The GOM inflow ratio was calculated according to Hebert et al. (2018):

$$Inflow\ Ratio = \frac{Nova\ Scotia\ transport}{Northeast\ Channel\ transport + Nova\ Scotia\ transport}$$

Stratification was defined as the difference in potential density between 100m and the surface (Alexander et al., 2020), except for locations shallower than 100m, where the bottom potential density was used.

2.5.2 Biological Analyses

P. australis growth potential was estimated according to the method in Clark et al. (2021). In short, growth rates were measured at 7, 9, 11, 13, and 15℃ for a *P. australis* isolate from the 2016 GOM bloom and extrapolated beyond the 7–15℃ temperature range according to a rate of

change of growth rate with temperature from short-term exposure experiments ($^{d\mu}/_{dT}$ = -0.02 $d^{-1}{}^{o}C^{-1}$ if T<7°C and -0.03 $d^{-1}{}^{o}C^{-1}$ if T>15°C). A theoretical curve was fit to the measured and estimated data points according to equation S.1 in Thomas et al. (2012). The growth curve, which agrees well with the literature (Thomas et al., 2012), is given in Figure 3, and the reader is referred to Clark et al. (2021) for more details. For each grid cell at each time step, a temperature-based potential growth rate was calculated by interpolating the simulated temperature to the growth curve. Many other factors can affect cellular abundance and growth, such as intraspecific variability or nutrient and light availability, but this analysis was intended to focus on the effects of temperature differences on *P. australis* growth. Therefore, the other factors are assumed to be non-limiting, and hereafter the "temperature-based potential growth rate" will be referred to as "potential growth rate" for brevity. Potential growth rate was calculated both for SST and for 10m temperatures because *P. australis* and DA have been observed at both depths in the GOM (Clark et al., 2019).

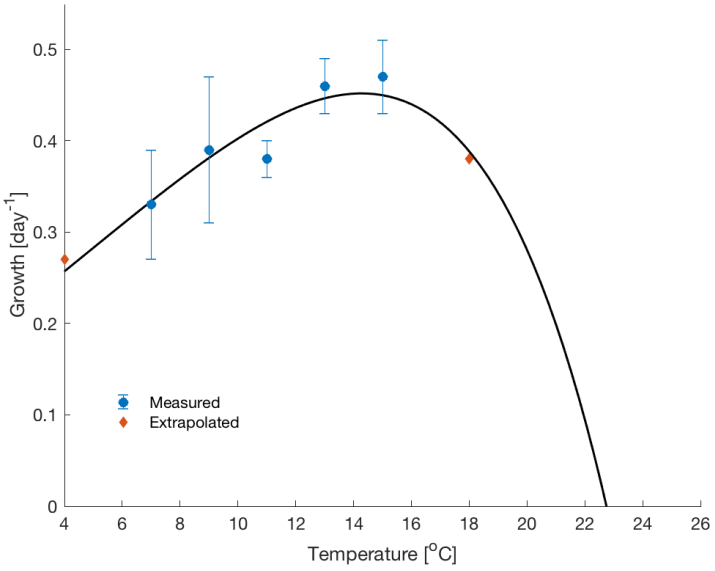

Figure 3. P. australis *growth vs. temperature as described in Clark et al. (2021). Values measured in laboratory experiments are marked with blue circles (error bars indicate standard error), while values that were extrapolated from short-term exposure experiments (see description in text) are indicated with orange diamonds. The black line indicates the growth curve that was fit according to the equation S.1 in Thomas et al. (2012). The growth curve is interpolated only as low as 4°C because laboratory equipment did not allow for measurement of growth rates below that temperature.*

The growing season was estimated as the number of days when average noon-time growth rates were greater than 75% of the maximum growth rate (appx 0.47 day^{-1} see Figure 3), according to Gobler et al. (2017). Surface noon-time growth rates were smoothed over a weekly time period before growing season analysis, because the "composite year" approach and associated averaging used here are more appropriate to assess weekly changes in growth than daily changes. An alternative approach for estimating growing season as a function of temperature is to define the HAB Window of Opportunity, as described for *A. catenella* in Puget Sound (Moore et al., 2011). This was deemed overly simplistic for *Pseudo-nitzschia* because there are multiple species, species might have different sources such as introduction or retention, and the same species has been found to grow in different temperature ranges depending on the location (e.g. *P. australis* in Clark et al. 2019; McCabe et al. 2016; Santiago-Morales and García-Mendoza, 2011; Thorel et al. 2014).

2.5.3 Averaging Data Spatially and Temporally

Model output was averaged both spatially and temporally to focus the analysis on regions and time periods of interest. A "composite year" is a year in which data were averaged across all 25 years from each simulation to represent the average hindcast or projection. Seasonal averages were broken down into winter (December to February), spring (March to May), summer (June to August), and fall (September to November). Regardless of whether data were averaged across the seasons, across the entire year, or averaged into composite years, a "change" in some parameter indicates the projected value minus the hindcast value (not to be confused with "Deltas" for the model forcing). Seasonal averages were calculated for the changes in SST, surface salinity, stratification, and *P. australis* potential growth.

To quantify interregional variability within the GOM ROMS domain, four sub-regions (Figure 2) were selected for spatial averaging. The Scotian Shelf was chosen because of its influence on the GOM interior via Scotian Shelf Water inflows, the Bay of Fundy was selected because it is where the 2016 *P. australis* bloom was first observed (Clark et al., 2019), the eastern Maine coast was selected because multiple DA-induced shellfishery closures have occurred here since 2016, and the GOM interior was chosen to assess internal dynamics over the deep basins. Changes in *P. australis* potential growth and growing season were averaged over these sub-regions.

3 Results

3.1 Hydrodynamics

3.1.1 Sea Surface Temperature

In the GOM ROMS projection, across the domain, SST increased by 2℃ on average, with the maximum increase in August and September. This agrees with the NWA ROMS projection in magnitude and seasonality. The average increase across the domain was 1.8℃ in winter, 1.9℃ in spring, 2.2℃ in summer, and 2.0℃ in fall. The seasonal signal and trend were consistent regardless of sub-region, but the magnitude of warming varied between regions. The Scotian Shelf had the greatest warming (up to 2.7℃ in August), while the Bay of Fundy had the least (maximum 1.9℃) (Figure 4). SST in the coastal regions (shallower than 50m) increased less than in the interior, regardless of season.

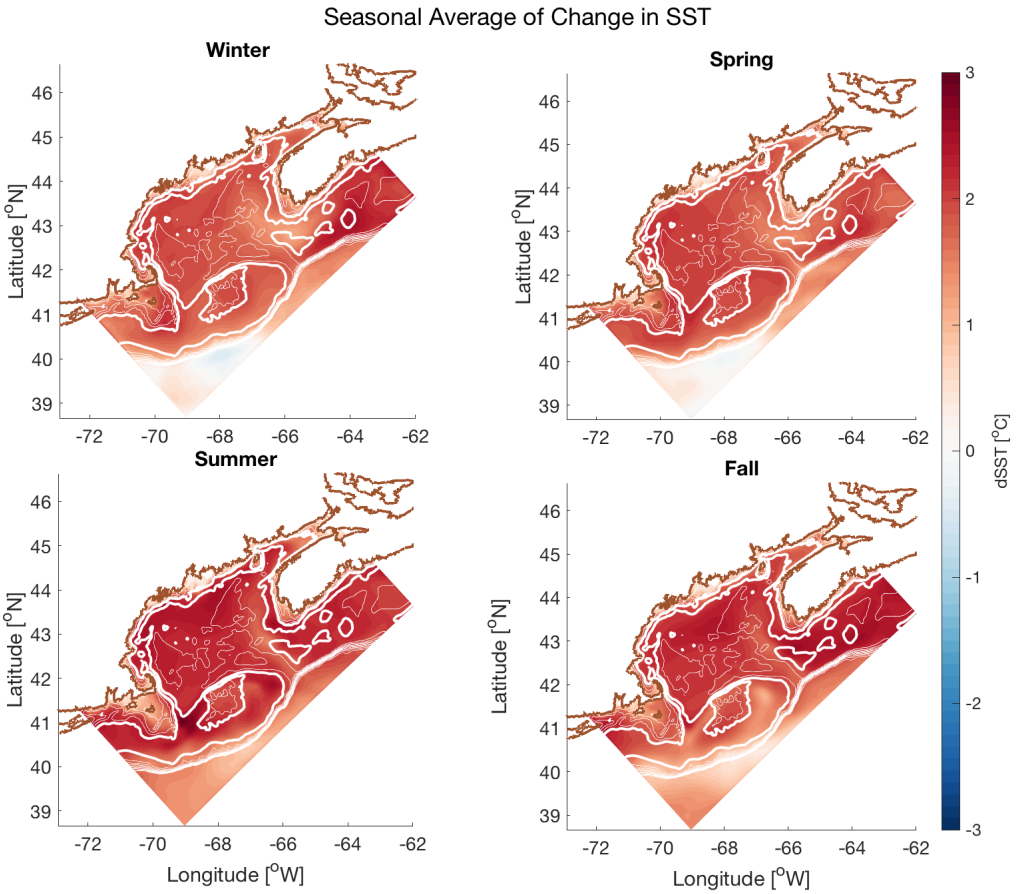

Figure 4. Seasonally-averaged change in SST in the (clockwise from top left) winter, spring, fall, and summer. Color values are defined by the color bar on the right. Bathymetry is drawn every 25m to 100m, every 100m to 1000m, and at 2000m and 3000m.

3.1.2 Surface Salinity

Surface salinity decreased throughout the GOM ROMS domain by 0.9 PSU on average (Figure 5). Although the seasonal signal was largely consistent between sub-regions, the degree of freshening varied. Salinity decreased between 0.8 and 1.1 PSU in the Bay of Fundy, GOM, and eastern Maine sub-regions, with the largest decrease occurring in the fall. On the Scotian Shelf, surface salinity decreased between 0.2 and 0.7 PSU, with the largest decrease in August.

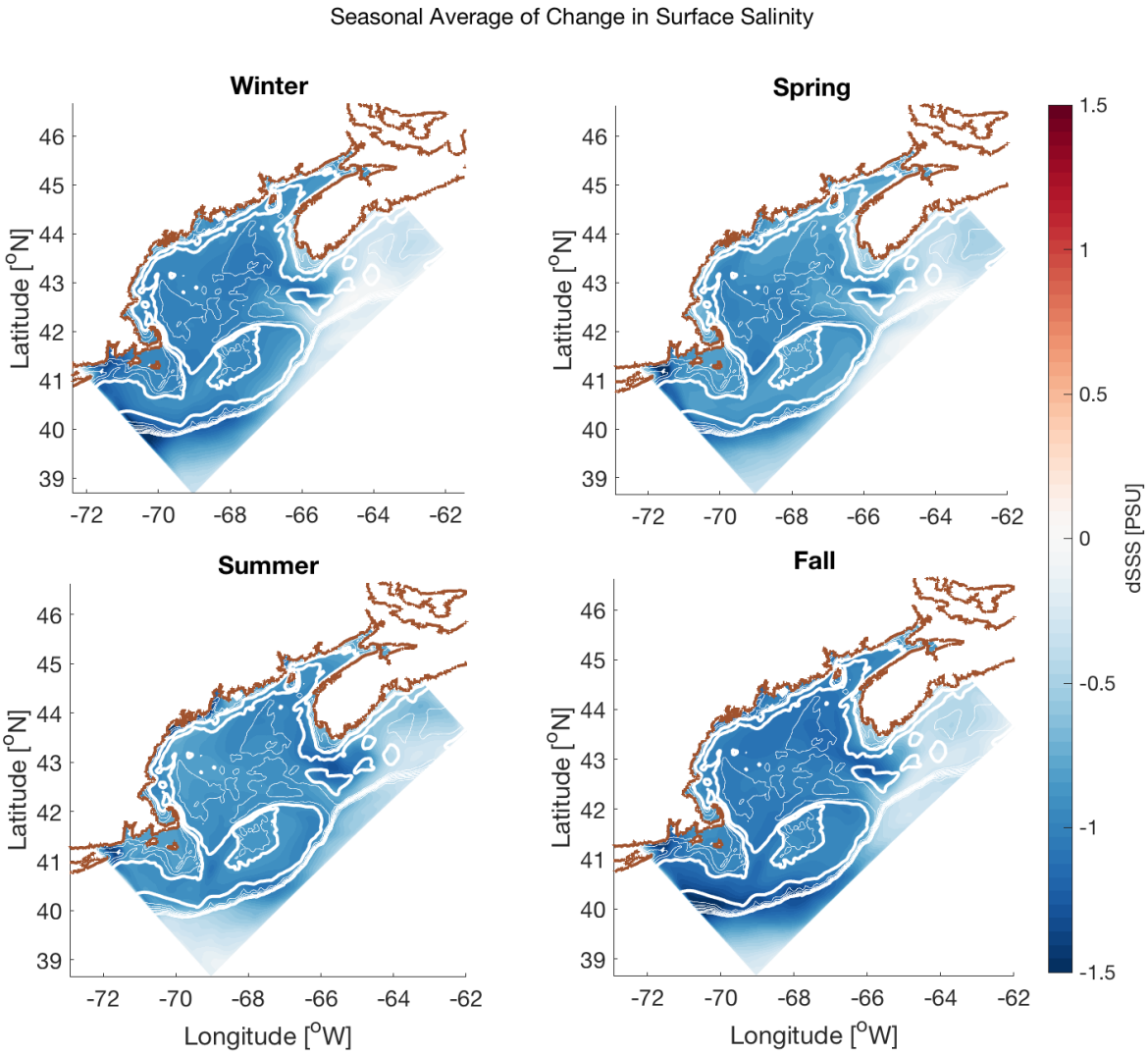

Figure 5. Seasonally-averaged change in surface salinity in the (clockwise from top left) winter, spring, fall, and summer. Color values are defined by the color bar on the right. Bathymetry is drawn every 25m to 100m, every 100m to 1000m, and at 2000m and 3000m.

3.1.3 Stratification

Stratification largely increased in the GOM ROMS projection throughout the domain, with interregional variability (Figure 6). Near the coast, in the Bay of Fundy, and at the crest of Georges Bank and Browns Bank, stratification increased only slightly, even in the summer. In contrast, in the GOM interior and offshore, stratification increased year-round in the projection by up to 3 kg m^{-3}. Regardless of interregional variability, the largest stratification increases generally occurred in the summer and fall.

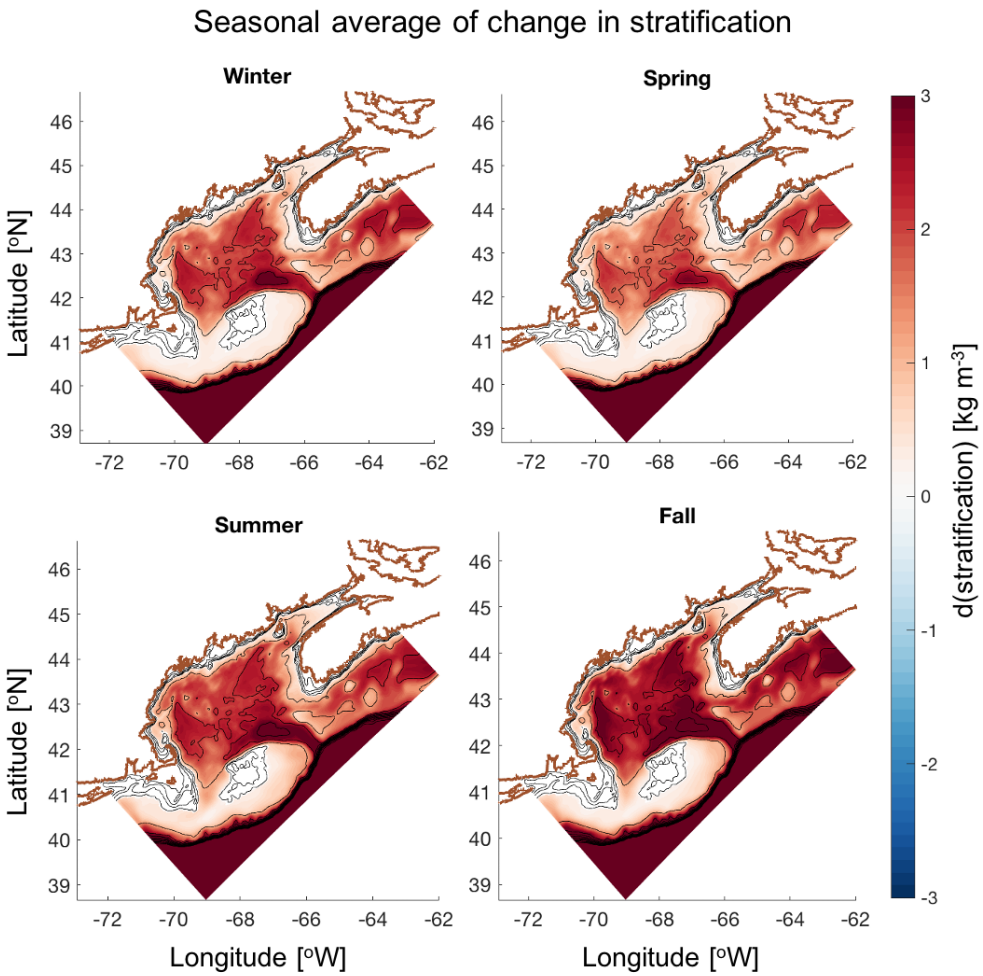

Figure 6. Seasonally-averaged change in stratification in the (clockwise from top left) winter, spring, fall, and summer. Color values are defined by the color bar on the right. Bathymetry is drawn every 25m to 100m, every 100m to 1000m, and at 2000m and 3000m.

3.1.4 Gulf of Maine Inflow Ratio

The Gulf of Maine inflow ratio increased year-round in the GOM ROMS projection, indicating increased inflow through the Scotian Shelf relative to inflows through the Northeast Channel. There was no discernible seasonal variability in this change. In the hindcast the ratio was approximately 0.5 on average, indicating that 50% of the inflows came via the Nova Scotia coastal route, which agrees with the results presented in Hebert et al. (2018). In the projection the inflow ratio increased by 0.1 on average, or 20% of the ratio in the hindcast (Supplementary Material Figure S-1), the drivers of which are discussed in Section 4.1.2. Both the GOM ROMS and the NWA ROMS projected an increase in the GOM inflow ratio (Supplementary Material, Figure S-2). The mean increase in the GOM ROMS was larger than the mean increase in the NWA ROMS, the likely cause of which is discussed in Section 4.1.1.

3.1.5 Eastern Maine Coastal Current

In the projection, alongshore transport in the EMCC decreased by 5% on average in the winter and spring and increased by 5% on average in the summer and fall (Figure 7). The result of this was an intensified seasonal signal, with the greatest increase (17%) occurring in mid-September. When the increase in total transport peaked, the projected alongshore velocity increased by about 2 cm s^{-1} over the hindcast.

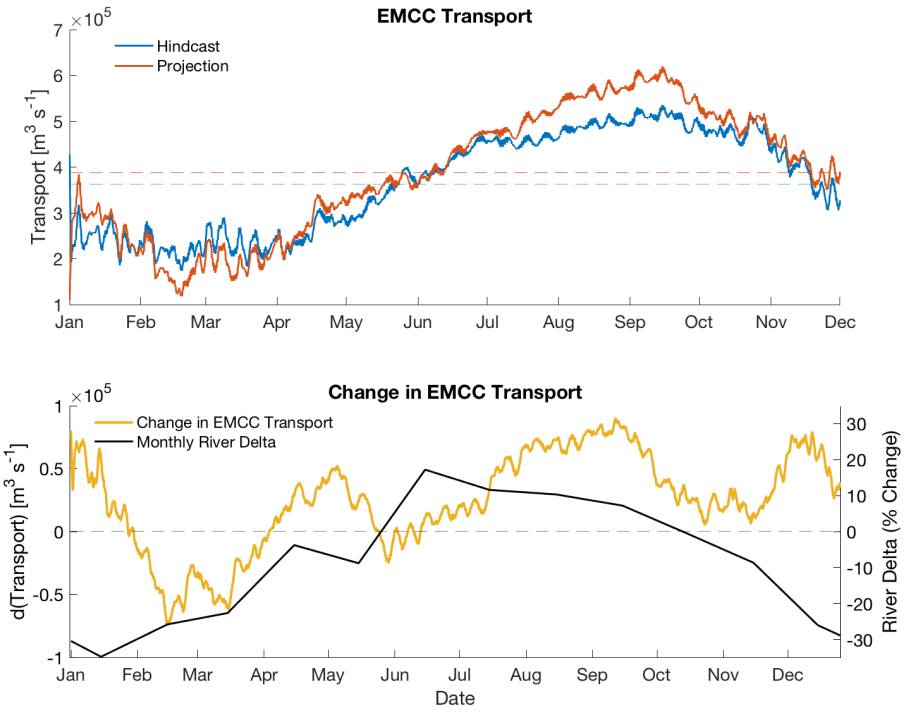

Figure 7. (top) Alongshore EMCC transport from the hindcast composite year (blue) and the projected composite year (red) vs. day of the year. Dashed lines in corresponding colors indicate the year-long average. (bottom) Change in alongshore EMCC transport vs. day of the year (yellow, left y axis), and monthly river delta as a percent change for each month (black, right y axis). EMCC data were smoothed over a weekly time period before plotting.

3.2 Projected Changes to *Pseudo-nitzschia* Growth

3.2.1 Growth Potential

In most of the GOM ROMS domain, average *P. australis* potential growth rates increased from November to June and decreased from June to November, with a maximum winter/spring increase of 0.17 day^{-1} in the Bay of Fundy and a maximum summer/fall decrease of 0.07 day^{-1} on the Scotian Shelf (Figure 8). However, there was interregional variability. In the interior GOM sub-region, the springtime increase stretched from February to March, while the Scotian Shelf, Bay of Fundy, and Eastern Maine sub-regions exhibited early and late spring peaks. The summertime decreases were larger in the GOM and Scotian Shelf sub-regions than in the Bay of Fundy and Eastern Maine sub-regions. The seasonal pattern of change in potential growth was similar at 10m, but the summertime decrease was less than at the surface, reflecting cooler temperatures at depth. In the Eastern Maine and Bay of Fundy sub-regions, potential growth at 10m did not decrease at any point in the summer (Figure 8).

Averaged seasonally, the change in growth potential in most sub-regions was positive in winter and spring and negative in summer and fall (Figure 9). Exceptions to this are found in shallow and tidally energetic regions, including the crest of Georges Bank, the shelf south of Nova Scotia including Browns Bank, the Bay of Fundy, and the eastern coast of Maine, where the spatially and temporally averaged change in growth potential at the surface was greater than zero in the winter and spring and approximately zero in the summer and fall.

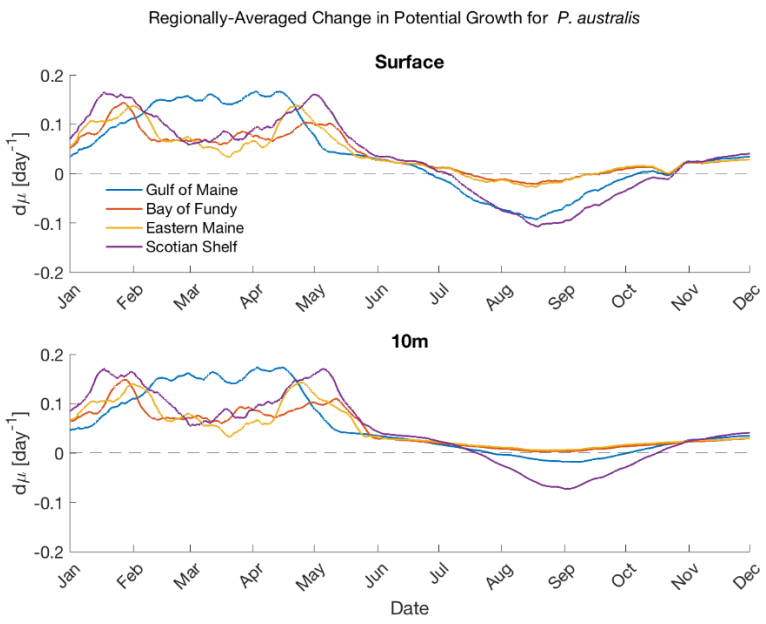

405

406 *Figure 8. Change in potential growth for each of the four sub-regions vs. time at the surface (top) and at 10m*
407 *(bottom). To see interannual variability in the projected changes in growth potential, refer to Figure S-3 and Figure*
408 *S-4 in the Appendix.*

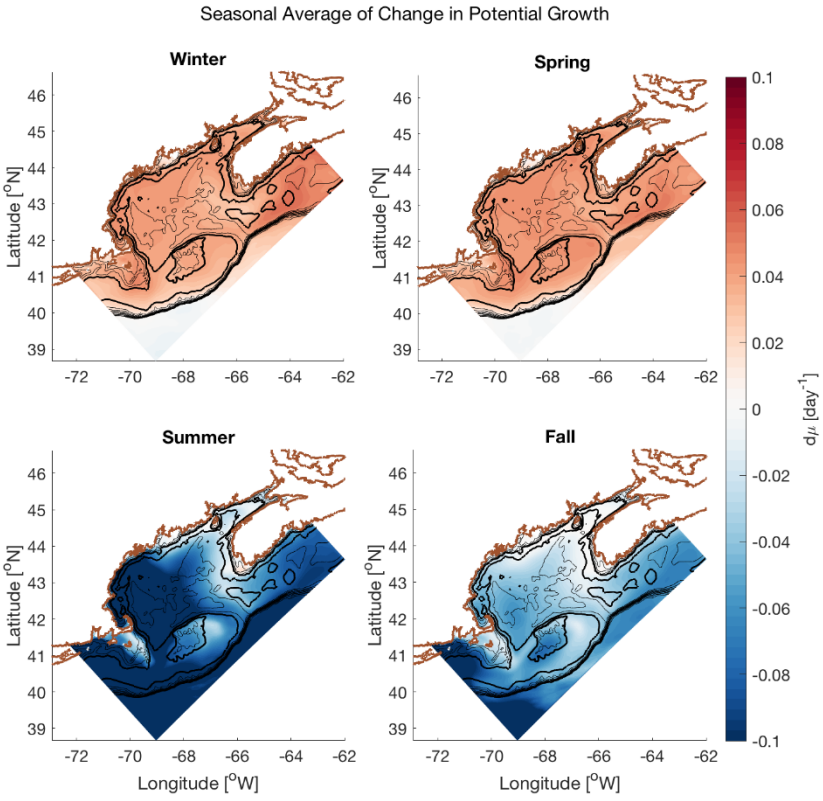

409

410 *Figure 9. Average change in surface* P. australis *potential growth in the GOM ROMS domain in the (clockwise from*
411 *top left) winter, spring, fall, and summer. Color values are given by the color bar on the right.*

3.2.2 Growing Season

The number of days in the *P. australis* growing season increased significantly in the projection for the Bay of Fundy by 3 weeks. Changes in growing season averaged over the Eastern Maine Coast, GOM, or Scotian Shelf sub-regions were not significant according to the Wilcoxon rank sum test, which tests the null hypothesis that the data in two samples are from distributions with the same median. When the year was divided into spring and fall growing seasons (i.e. the first half and second half of the year), it became apparent that the growing season increased significantly only in the first half of the year. The spring growing season increased significantly by 4–6 weeks in all sub-regions, while the fall growing season decreased significantly by 6–7 weeks in the GOM and Scotian Shelf sub-regions. Significant changes in growing season for each sub-region are summarized in Table 1.

Table 1. Change in growing season in days averaged over each of the sub-regions. Only numbers that are significant at the 95% confidence level are listed. The difference is given in days in the table but rounded to the nearest week in the text.

Sub-Region	Annual Growing Season dt (days)	Spring Growing Season dt (days)	Fall Growing Season dt (days)
Gulf of Maine	--	+40	-43
Scotian Shelf	--	+40	-51
Bay of Fundy	+23	+36	--
Eastern Maine Coast	--	+28	--

4 Discussion

4.1 Mechanisms Behind Changing Hydrodynamics

4.1.1 Sea Surface Temperature, Surface Salinity, and Stratification

The general trend in SST – warming overall and enhanced warming in the summer – was also noted in Alexander et al. (2020) and in the GFDL-ESM2M. This is partially explained by a positive feedback between summer warming and stratification: surface warming leads to increased stratification, which leads to reduced mixing with cooler, deeper waters, stronger air-sea temperature coupling, and a shallower layer over which to distribute the heat flux (Alexander et al., 2020, 2018; Thomas et al., 2017b). Warming was stronger on the Scotian Shelf than in other sub-regions (Figure 4), which could be caused both by enhanced warming at northerly latitudes

as shown in the GFDL-ESM2M output (Alexander et al., 2020), and by the warming-stratification feedback. In contrast, the Bay of Fundy and Eastern Maine sub-regions, although at similar latitudes to the Scotian Shelf sub-region, had amongst the smallest changes in SST (Figure 4). This is likely the result of strong vertical mixing by the tides, which transports deep, cooler waters to the surface.

Surface salinities decreased throughout the domain in the projection, with the largest decrease in late summer and in the GOM interior (Figure 5). This agrees with projections for the GOM in other studies (Brickman et al., 2021). Decreased salinity was the result of increased freshwater transport into the domain at the eastern and southern boundaries. Freshening north of 40°N occurred in the GFDL-ESM2M, with stronger freshening in summer than in winter (Alexander et al., 2020) because of sea ice melt and an increase in precipitation relative to evaporation ($\Delta(E-P)<0$) in the Subpolar Gyre and Labrador Sea. This upstream freshwater was likely advected into the GOM (Alexander et al., 2020) via alongshore transport on the Scotian Shelf and shelf break. Some areas saw stronger freshening than average, especially areas of steep bathymetry such as Georges Bank (Figure 5), but this was simulated only by the GOM ROMS.

The GOM ROMS and NWA ROMS both projected freshening in the GOM, but they disagreed on the magnitude. Surface salinity decreased by 0.3 PSU on average in the NWA ROMS projection within the GOM ROMS domain, but by 0.9 PSU on average in the GOM ROMS projection (Supplementary Material, Figure S-3). This was largely a result of how the two models resolved alongshore transport at the GOM ROMS eastern boundary on the Scotian Shelf (Figure 10). At this boundary, the average salinity Delta was negative, with stronger freshening nearshore, and the average alongshore velocity Delta was positive (toward the GOM), with a maximum increase of 5 cm s^{-1} nearshore. Nearshore velocities toward the GOM were also, on average, 10 cm s^{-1} faster in the GOM ROMS hindcast than in the NWA ROMS hindcast. The freshwater transport toward the GOM was therefore larger in the GOM ROMS than the NWA ROMS. The enhanced freshening in the GOM ROMS occurred even though the average surface salinity at the GOM ROMS eastern boundary in the hindcast was greater in the GOM ROMS than in the NWA ROMS (Supplementary Material Figure S-4), which highlights the role of freshwater advection throughout the water column.

The refined resolution of coastal currents in the GOM ROMS may have amplified the increases in freshwater inflow apparent in the NWA ROMS. Alexander et al. (2020) also noted that salinity decreases were stronger and more spatially extensive in the NWA ROMS compared to the Global Climate Model. On average, freshwater transport at the eastern boundary increased by 11.46 mSv (1 Sv = 10^6 m^3 s^{-1}) in the GOM ROMS and by 2.81 mSv in the NWA ROMS, a difference of 8.65 mSV. The Arctic is the primary upstream freshwater source to the Scotian Shelf via the Labrador Sea, and the difference in freshwater transport between the GOM and NWA ROMS is only a small fraction of the projected increase in Arctic freshwater export estimated in the literature. For comparison, Han et al. (2019) projected that freshwater export from the Labrador Sea could increase nearly three-fold, from 110 mSv to 350 mSv, by the end of the 21st Century under a median emissions scenario. The difference between the GOM ROMS and NWA ROMS is only 4% of this increase. In addition, projections for future Arctic freshwater export vary widely, from 130 mSv (Haine et al., 2015) to 159 mSv (Vavrus et al., 2012), to 350 mSv (Han et al., 2019), although not all of these projections included present-day estimates for comparison. The difference in freshwater transport between the NWA and GOM ROMS is therefore relatively small compared to the greater uncertainty in the delivery of freshwater from upstream.

The difference between the GOM ROMS and NWA ROMS freshwater transport is also only one source of uncertainty in this study. Downscaled model results can vary based on the chosen global model (Alexander et al., 2020; Brickman et al., 2021; Drenkard et al., 2021) and Representative Concentration Pathway (Brickman et al., 2021). Drenkard et al. (2021) suggested downscaling an ensemble of GCMs to mitigate this uncertainty, which this study does not do. However, the changing temperature and salinity signals are robust despite the lack of an ensemble approach, for several reasons. First, the warming signal was consistent across the three models considered by Alexander et al. (2020) and, in the GFDL model, the warming pattern was only weakly impacted by additional resolution refinement. The freshening signal was less consistent across the three models tested in Alexander et al., but freshening on the whole is consistent with recent observational evidence suggesting increased Scotian Shelf Water inflows to the Gulf of Maine because of freshening in the Labrador Sea (Townsend et al., 2015). It also agrees with projected increases in high latitude precipitation in global climate projections (Collins

et al., 2013; Knutson and Zeng, 2018; Knutti and Sedláček, 2013). Future efforts with larger ensembles and downscaled hydrological models are needed to more fully constrain the range of projected circulation patterns and associated salinity changes.

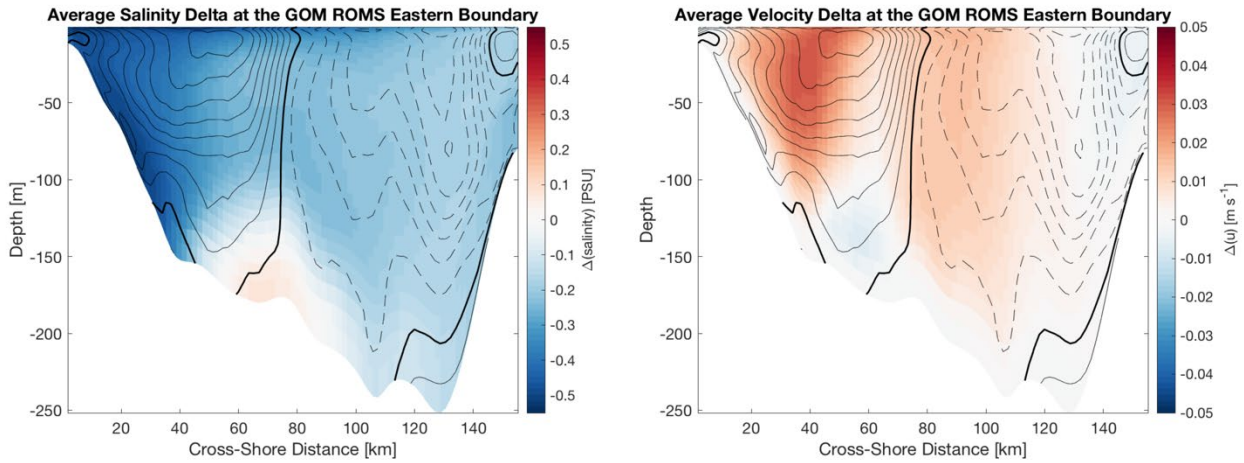

Figure 10. Colored contours of the average salinity Delta (left) and velocity Delta (right) at the GOM ROMS eastern boundary. Depth in meters is shown on the y axis, and cross-shore distance in km is shown on the x axis, with the coastline to the left. Corresponding color values are given in the color bars on the right. A positive velocity indicates flow toward the GOM. In both plots, contours of the difference in average hindcast velocity between the GOM ROMS and NWA ROMS are overlain in thin black lines. Solid contours indicate $u_{GOM\ ROMS} - u_{NWA\ ROMS} > 0$ *(i.e. GOM ROMS transport toward the GOM is stronger), while dashed contours indicate* $u_{GOM\ ROMS} - u_{NWA\ ROMS} < 0$ *(i.e. NWA ROMS transport toward the GOM is stronger). Contours are drawn every 0.02 m s^{-1}, and the zero contour is drawn with a thick black line.*

4.1.2 Scotian Shelf Inflows and the Gulf of Maine Inflow Ratio

The projected increased velocities (and consequently, transport) at the eastern boundary (Figure 10) help explain several changes downstream. First, they likely caused the increase in the GOM inflow ratio, because the increase was caused more by increased Scotian Shelf Water inflows than by decreased Northeast Channel inflows (Supplementary Material, Figure S-2). Second, the stronger alongshore transport in the GOM ROMS relative to the NWA ROMS (Section 4.1.1) explains the greater increase in the GOM inflow ratio in the GOM ROMS over the NWA ROMS. Third, because Scotian Shelf Water inflows are relatively cool compared to Northeast Channel inflows (Townsend et al., 2015), and because the inflows continue via the coastal current into the Bay of Fundy, increased Scotian Shelf Water inflows could help explain the relatively small increases in SST near the coast south of Nova Scotia, in the Bay of Fundy, and along eastern Maine. In both the hindcast and projected composite years, a mass of cool surface water enters the domain from the Scotian Shelf, wraps around Nova Scotia, and spreads into the Bay of Fundy,

similar to what has been seen in satellite images (Luerssen et al., 2005). In the projected composite year, while the average surface temperature in most of the domain was 16℃, this coastal region remained between 8 and 12℃ (Supplementary Material, Figure S-5).

4.1.3 Eastern Maine Coastal Current

The Eastern Maine Coastal Current (EMCC) has been shown to be an important driver of alongshore HAB dispersal in the GOM (Keafer et al., 2005; Li et al., 2009). The EMCC is driven by a pressure gradient that is influenced by several factors, including river outflow (Bisagni et al., 1996; Brooks, 1994; Keafer et al., 2005), Scotian Shelf inflows (Brooks, 1994; Lynch et al., 1997), and the volume and extent of dense slope water in the Jordan Basin (Brooks, 1994; Lynch et al., 1997). Enhanced Scotian Shelf inflows have been connected to increased EMCC transport (Brooks, 1994). This explanation seems unlikely to explain the presented results, however, because the GOM inflow ratio increased year-round, with no apparent seasonal variability (Figure S-1), while the EMCC transport decreased from February to June and increased from July to November.

Increased river discharge can also increase EMCC transport (Pettigrew et al. 2005). As shown in Figure 7, the projected enhancement of river flows associated with climate change (i.e. the Deltas) peaked in June, and was positive from mid-May to mid-September (Figure 7). EMCC transport increased in the projection from mid-July to mid-October. This 60-day lag between enhancement of river flow and enhanced EMCC transport is longer than the 45 day lag between the St. John River and Penobscot Bay that was suggested by Brooks (1994). The lags are of a similar order of magnitude, however, suggesting that river outflow is a reasonable explanation for the increase in transport. An important caveat is that the expected changes in river outflow with climate change are not agreed upon for this region: while most studies find that river discharge is expected to decrease at low latitudes and increase at high latitudes with climate change, they disagree on whether the GOM corresponds to a “high latitude” or “low latitude” regime (e.g. Arnell, 1999; Gosling et al., 2017, 2011; Prudhomme and Davies, 2009).

4.2 *P. australis* Potential Growth

The temporal and spatial variability in predicted *P. australis* potential growth is driven directly by the variability in ocean temperatures. Temperatures in winter and spring were below the

temperature of peak growth (0.45 day^{-1} at approximately 15℃, see Figure 3) in the hindcast and warmed toward peak growth temperatures in the projection. In contrast, temperatures in summer and fall were near to or greater than the peak growth temperature in the hindcast and became too warm in the projection. This happened throughout the domain, as shown in Figure 8 and Figure 9. The effects of warming on growth rate were smallest in the Bay of Fundy and Eastern Maine Coast sub-regions because the combination of strong tidal mixing, northerly latitude, and relatively cool inflows from the Scotian Shelf kept temperatures in the species' optimal range of 11–15℃. This explains why seasonally averaged growth potential increased or was unchanged in all seasons in these sub-regions but nowhere else in the domain (Figure 9).

Although projected potential growth rates at the surface decreased in every sub-region in summer, the effect diminished with depth. In the Bay of Fundy and Eastern Maine Coast sub-regions, 10m potential growth rate did not change (Figure 8) in the summer. This is logical, because sub-surface waters are typically cooler than surface waters and less affected by atmospheric warming and solar radiation, depending on the mixed layer depth. It is also important, because sub-surface *P. australis* populations have been found to seed *Pseudo-nitzschia* blooms off the coasts of Ireland (Cusack et al., 2015), Washington state (Trainer et al., 2000), and Southern California (Seegers et al., 2015). Just because the surface becomes too warm does not mean that the environment will become inhospitable to *P. australis*; sub-surface populations that are deep enough to be in cooler water but shallow enough to be in the euphotic zone may become more prevalent in seeding future blooms.

Light and nutrient availability might also affect *P. australis* blooms in the future, but neither of these parameters are addressed by a simple model of growth based on temperature. In the projection, *P. australis* growth potential increased in the spring, when nutrients are typically abundant and light is limiting until March, and the late fall, when nutrients are typically depleted and light is limiting after September. Therefore, a new or extended spring niche for *P. australis* blooms in April or May seems more likely than an expanded fall niche in late October or November. However, *P. australis* has bloomed in October and November in the GOM since 2016, suggesting that limited light and nutrient availability do not prevent its survival; this is also the time frame when conditions become more favorable for growth in the projection.

4.3 *P. australis* Domoic Acid Production

Domoic Acid production is a complex and poorly understood process. Laboratory studies have shown *Pseudo-nitzschia* toxicity to be affected by copper exposure (Fuentes and Wikfors, 2013; Maldonado et al., 2002), growth phase (Davidson and Fehling, 2006; Tammilehto et al., 2015; Terseleer et al., 2013), pH (Lundholm et al., 2004) and silicate or iron limitation (Maldonado et al., 2002; Terseleer et al., 2013). In the field, DA concentrations have correlated with low silica-to-nitrogen ratios (Marchetti et al., 2004), but many field studies have been inconclusive (Hardardóttir et al., 2015; Tammilehto et al., 2015). In addition, DA production can vary between species (Lema et al., 2017) and species strains (Fehling et al., 2004b). It is thus a difficult process to predict in the present day, let alone at the end of the 21st Century.

Despite the ambiguities surrounding DA production, however, some studies have explored the potential effects of a changing climate on *Pseudo-nitzschia* toxicity. Zhu et al. (2017) found that DA production by a *P. australis* isolate from the 2015 bloom on the U.S. West Coast (McCabe et al., 2016; McKibben et al., 2017) increased with temperature, peaking at 30°C. Thorel et al. (2014) found that DA production by a *P. australis* isolate from the English Channel increased with growth rate, which also increased with temperature. There is therefore precedent that increasing temperatures could increase *P. australis* toxicity in the Gulf of Maine as well, as long as the temperatures remain within the preferred range for growth. There are complicating factors, however, because changing temperatures could also shift the timing of DA production. This could affect the influence of nutrient ratios and predatory pressure, both of which have been shown to induce DA production (Lema et al., 2017; Lundholm et al., 2018), thereby negating or exacerbating the effect of changing temperature. These potential changes are purely speculatory and warrant future research.

4.4 *P. australis* in the Eastern Gulf of Maine

The predicted changes to hydrodynamics and *P. australis* growth potential, when combined, suggest that *P. australis* blooms in the eastern GOM may intensify in the latter half of the 21st Century. First, Clark et al. (2021) established that the most likely introduction pathway of *P. australis* to the GOM in 2016 was from the inner Scotian Shelf via the coastal current south of Nova Scotia. Assuming an established upstream population of *P. australis*, increased transport from the Scotian Shelf would increase the delivery of cells to the Bay of Fundy. In addition, Scotian

Shelf inflows typically have a silica-to-nitrogen ratio greater than 1, which can support a diatom community (Townsend et al., 2010) and increase the likelihood of a bloom in the Bay of Fundy. A greater silica-to-nitrogen ratio might contribute conversely to decreased DA production, however, which is often associated with low silica-to-nitrogen ratios (Lema et al., 2017; Tatters et al., 2012; Terseleer et al., 2013). Second, average potential growth rates increased from fall to early spring in the eastern GOM, the same time and place of past *P. australis* blooms. The seminal 2016 DA event, for example, occurred in September and October along the eastern Maine coast (Clark et al., 2019), and, since 2016, *P. australis* cells have bloomed each year in eastern Maine in the late fall (Chadwick, 2021). Finally, increased EMCC transport in the fall might affect a *P. australis* bloom's distribution. The EMCC is known to contribute to the alongshore extent of HABs in the GOM (Anderson et al., 2005; Townsend et al., 2001), and strengthened alongshore transport might carry *P. australis* cells from the eastern GOM to the west. This hypothesis should be the subject of future monitoring efforts and research.

4.5 *Pseudo-nitzschia* Community Composition

P. australis is not the only *Pseudo-nitzschia* species in the GOM: there are currently 15 known species in the region (Clark et al., 2019; Fernandes et al., 2014), some of which (such as *P. plurisecta* and *P. seriata*) are known DA producers. There are several examples of shifts in species composition in response to changing environmental factors on event (Schnetzer et al., 2013, 2007), seasonal (Chadwick, 2021; Fehling et al., 2006; Thessen and Stoecker, 2008), interannual (Clark et al., 2019), and decadal (Lundholm et al., 2010; Parsons et al., 2002) time scales, so it is important to consider how the species assemblage might change as a result of climate change.

To consider an envelope of variability, *P. australis* was compared to a representative "cold-adapted" species and a representative "warm-adapted" species, both of which already exist in the GOM *Pseudo-nitzschia* species assemblage. *P. seriata* has been shown to grow in -2 to 12℃, with a lethal limit between 12–15℃ (Smith et al., 1994), and is the representative cold-adapted species. *P. plurisecta* is the representative warm-adapted species because it typically blooms in the GOM in July and August and dominated the species assemblage at 15.5–16℃ in 2013 (see Figure 3 in Clark et al., 2019). To estimate changes in these species' potential growth in the

projected GOM, the *P. australis* growth curve was shifted such that growth approached zero at 15℃ for *P. seriata* and peaked at 17℃ for *P. plurisecta* (Supplementary Material, Figure S-6). The same analyses of potential growth and growing season were then calculated. This approach does not seek to understand how all species in the *Pseudo-nitzschia* assemblage might change, but rather to represent an envelope of variability. The full growth rates as a function of temperature for the GOM strains of *P. plurisecta* and *P. seriata* are not known, so this is only an approximation for species whose growth curves peak at higher or lower temperatures. Measured growth rates for *P. seriata* isolated from 15℃ Scottish waters were approximately 0.55–0.58 day^{-1} in a study by Fehling et al. (2004), which is similar to the maximum growth rate for *P. australis* (0.47 day^{-1}) described in Clark et al. (2021). Growth rates for *P. plurisecta* are not currently available in the literature.

In the projection, the cold-adapted species' growth potential decreased from May through January, with a slight increase from February through April (Figure 11), and its growing season contracted significantly by 3–6 weeks in each sub-region (Table 2). This is because the projected GOM became too warm for the cold-adapted species, decreasing its ability to grow without further adaptation. Meanwhile, time periods previously too cold for the warm-adapted species became more hospitable, its potential growth increased in parts of the summer (Figure 11), and its growing season in the Bay of Fundy and Eastern Maine Coast sub-regions increased significantly by 4 weeks (Table 2). Average temperatures increased into the warm-adapted species' growing window, and its growing season lengthened by moving into the spring and fall. In the eastern GOM, *P. australis'* projected growing season shifted to replace the cold-adapted species, while it was replaced by the warm-adapted species in its present bloom periods. This suggests that niches might open in both spring and early fall for blooms of species that previously only bloomed in the summer in the GOM, while niches may close for cold-adapted species.

These predictions all rely on a growth curve for a single isolate of *P. australis*, which was shown to be similar to other growth curves from the literature (Clark et al., 2021). However, different *Pseudo-nitzschia* species in the GOM and their intraspecific variants might thrive in a variety of temperatures, and new species or strains may be introduced over time. As temperatures increase, it is possible that populations more suited to the warmer temperatures could out-

compete cold-adapted ones, such that shifts occur primarily between strains instead of – or in addition to – between species. For example, a warm-adapted strain of *P. australis* might bloom in the future, rather than *P. plurisecta.* These predictions should therefore be treated with caution as an example of what might happen in the future.

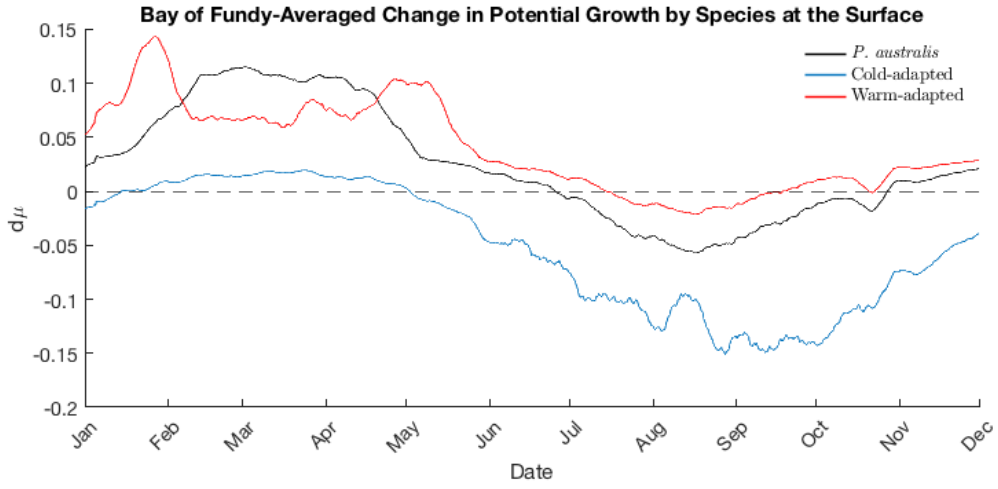

Figure 11. Change in growth potential at the surface averaged over the Bay of Fundy vs. time for (black) P. australis*, (blue) the cold-adapted species, and (red) the warm-adapted species. The Bay of Fundy was chosen as an illustrative sub-region because of its relevance to* P. australis *blooms in the GOM and because it was one of only two sub-regions where change in growing season was significant for all three species.*

Table 2. Change in growing season (days) for P. australis *and the representative cold-adapted and warm-adapted species. Only numbers that were significant at the 95% confidence level are shown. Note that values are given in days in the table and listed as weeks in the text.*

Sub-Region	***P. australis*** Season dt (days)	Cold Species Season dt (days)	Warm Species Season dt (days)
Gulf of Maine	--	-37	--
Scotian Shelf	--	-27	--
Bay of Fundy	+24	-31	+28
Eastern Maine	+19	-39	+26

4.6 Effects of Physical Changes on Phytoplankton Functional Groups

Pseudo-nitzschia species are not the only phytoplankton present in the GOM, and any projected changes, such as to stratification strength and timing, will likely affect other planktonic functional groups as well. Early stratification onset could lead to an earlier spring bloom (Song et al., 2011;

683 Sverdrup, 1953), which could affect DA production or deplete nutrients before *Pseudo-nitzschia*
684 can grow. This phenomenon has occurred in the GOM and partly explains the suppression of the
685 annual *A. catenella* bloom in 2010 (McGillicuddy et al., 2011, see Section 4.6). Increases in
686 stratification may also be unfavorable to diatoms (Bopp et al., 2005; John et al., 2015), despite
687 the fact that long-term warming has been shown to contribute to shifts in the phytoplankton
688 assemblage toward diatoms and away from dinoflagellates (Hinder et al., 2012). Diatoms
689 (including *Pseudo-nitzschia*) are typically competitive in turbulent, eutrophic waters because they
690 have faster growth rates under high nutrient concentrations (Miller and Wheeler, 2012), but their
691 inability to swim and their hard silica shells necessitate a physical transport process to return
692 them to the surface (Miller and Wheeler, 2012).

693 Increased stratification might suppress wind-induced vertical mixing and reduce the introduction
694 of new nutrients from deeper waters, which presents a challenge to the entire phytoplankton
695 community (Doney, 2006). Dinoflagellates might be more competitive than diatoms in this
696 environment because they can migrate vertically to access nutrients. *Pseudo-nitzschia* might
697 have an advantage relative to other diatoms, however, because they are smaller and lightly
698 silicified, so do not require as much silica (Marchetti et al., 2004; Parsons et al., 2002). Whether
699 that advantage is enough to overcome the disadvantages of negative buoyancy and immobility
700 remains to be seen, especially considering the strong tidally induced mixing in the nearshore
701 GOM. Increased stratification with climate change in the global oceans will have different
702 consequences depending on the latitude and phytoplankton in question (Anderson, 2014;
703 Hallegraeff, 2010; Moore et al., 2008; Wells et al., 2020), and a complete understanding of *P.*
704 *australis* bloom dynamics in the future will require a deeper investigation of how it interacts with
705 the planktonic ecosystem in which it is embedded, including top-down controls (Banse, 1992).

706 ## 4.7 Variability and Episodic Events in the Context of Long-Term Change

707 This study has focused on mean changes in hydrodynamics, temperature, and *Pseudo-nitzschia*
708 potential growth, but variability and episodic events superimposed on the mean change are also
709 important. Events such as the Warm Blob on the U.S. West Coast (McCabe et al., 2016; Ryan et
710 al., 2017; Trainer et al., 2020) and marine heat waves in the GOM (Pershing et al., 2018, 2015)
711 have caused extreme *Pseudo-nitzschia* blooms and fisheries collapses, respectively. In 2010 in

the GOM, because of several simultaneous departures from typical conditions, the annual *A. catenella* bloom did not occur despite large cyst abundance portending a large bloom (McGillicuddy et al., 2011). First, abnormally warm and fresh surface waters led to early onset of stratification, an early spring bloom, and depletion of nutrients in surface waters. The resulting mismatch in nutrient availability and *A. catenella* germination suppressed the bloom. Second, strong upwelling-favorable winds reduced alongshore transport via the Maine Coastal Current, limiting the downcoast transport of cells (McGillicuddy et al., 2011). These simultaneous changes in hydrodynamics are an example of how the mean shift alone might not tell the whole story; concurrent changes in multiple factors can alter bloom dynamics or suppress a bloom entirely. Some of the factors that suppressed the 2010 *A. catenella* bloom, such as warm, fresh surface waters and earlier stratification onset, are predicted to increase with climate change, potentially increasing the occurrence of such events in the future.

5 Conclusions

In this study, the Delta Method was used to downscale climate simulations to a 1–3-km-resolution GOM ROMS and to simulate the effects of climate change on *Pseudo-nitzschia* growth potential in the GOM. Output was analyzed for changes to SST, surface salinity, stratification, inflows, transport, and *P. australis* potential growth and growing season. On average, the GOM is projected to warm by 2℃, freshen by 0.9 PSU, and become more stratified by 3 kg m^{-3}. The relative strength of Scotian Shelf inflows to the GOM may increase by as much as 20% in the future, and autumnal transport in the Eastern Maine Coastal Current may strengthen by up to 20%. In the climate simulations, as a result of increased SST, *P. australis* surface potential growth increased throughout the domain from November to June and decreased in most of the domain from June to November, due to warming that exceeded the optimal temperature for growth. Sub-surface growth rates did not decrease as much as surface growth rates in the projection due to more moderate temperature increases. As a result of changing potential growth rates, blooms are likely to shift later in the fall and are more likely to persist through winter into spring. As the timing and duration of *P. australis* blooms change, so might the GOM *Pseudo-nitzschia* community composition: cold-adapted species and populations are likely to become less prevalent, while warm-adapted species and populations might fill the seasonal niche previously

dominated by *P. australis* and species in the same temperature range. A more complete assessment of *Pseudo-nitzschia* bloom dynamics will require explicit treatment of both bottom-up and top-down controls on these populations, as well as interactions with the plankton ecosystem of which they are a part.

Acknowledgements

This research was funded by the National Science Foundation (Grant Number OCE-1840381), the National Institute of Environmental Health Sciences (Grant Number 1P01ES028938), the Woods Hole Center for Oceans and Human Health, and the Academic Programs Office of the Woods Hole Oceanographic Institution.

6 Bibliography

Alexander, M.A., Scott, J.D., Friedland, K.D., Mills, K.E., Nye, J.A., Pershing, A.J., Thomas, A.C., 2018. Projected sea surface temperatures over the 21st century: Changes in the mean, variability and extremes for large marine ecosystem regions of Northern Oceans. Elem. Sci. Anthr. 6.

Alexander, M.A., Shin, S.-I., Scott, J.D., Curchitser, E., Stock, C., 2020. The Response of the Northwest Atlantic Ocean to Climate Change. J. Clim. 33, 405–428. https://doi.org/10.1175/JCLI-D-19-0117.1

Anderson, D., 2014. HABs in a changing world: a perspective on harmful algal blooms, their impacts, and research and management in a dynamic era of climactic and environmental change. Harmful Algae 3–17.

Anderson, D.M., Keafer, B.A., McGillicuddy, D.J., Mickelson, M.J., Keay, K.E., Scott Libby, P., Manning, J.P., Mayo, C.A., Whittaker, D.K., Michael Hickey, J., He, R., Lynch, D.R., Smith, K.W., 2005. Initial observations of the 2005 Alexandrium fundyense bloom in southern New England: General patterns and mechanisms. Deep. Res. Part II Top. Stud. Oceanogr. 52, 2856–2876. https://doi.org/10.1016/j.dsr2.2005.09.004

Arnell, N.W., 1999. Climate change and global water resources. Glob. Environ. Chang. S31–S49. https://doi.org/10.1507/endocrj.42.83

Banse, K., 1992. Grazing, temporal changes of phytoplankton concentrations, and the microbial loop in the open sea., in: Primary Productivity and Biogeochemical Cycles in the Sea. Springer US, pp. 409–440.

Barron, J.A., Bukry, D., Field, D.B., Finney, B., 2013. Response of diatoms and silicoflagellates to climate change and warming in the California Current during the past 250 years and the recent rise of the toxic diatom Pseudo-nitzschia australis. Quat. Int. 310, 140–154. https://doi.org/10.1016/j.quaint.2012.07.002

Bates, S.S., Hubbard, K.A., Lundholm, N., Montresor, M., Leaw, C.P., 2018. Pseudo-nitzschia, Nitzschia, and domoic acid: New research since 2011. Harmful Algae 79, 3–43. https://doi.org/10.1016/j.hal.2018.06.001

Bigelow, H., 1927. Dynamic oceanography of the Gulf of Maine. Trans. Am. Geophys. Union 206–211. https://doi.org/10.1063/1.3058361

Bisagni, J.J., Gifford, D.J., Ruhsam, C.M., 1996. The spatial and temporal distribution of the Maine Coastal Current during 1982. Cont. Shelf Res. 16, 1–24.

Bopp, L., Aumont, O., Cadule, P., Alvain, S., Gehlen, M., 2005. Response of diatoms distribution to global warming and potential implications: A global model study. Geophys. Res. Lett. 32, 1–4. https://doi.org/10.1029/2005GL023653

Brickman, D., Alexander, M.A., Pershing, A., Scott, J.D., Wang, Z., 2021. Projections of physical conditions in the Gulf of Maine in 2050. Elem. Sci. Anthr. 9, 1–15. https://doi.org/https://doi.org/ 10.1525/elementa.2020.20.00055

Brooks, D.A., 1994. A model study of the buoyancy-driven circulation in the Gulf of Maine. Am. Meteorol. Soc. 2387–2412.

Carton, J.A., Giese, B.S., 2008. A reanalysis of ocean climate using Simple Ocean Data Assimilation (SODA). Mon. Weather Rev. 136, 2999–3017. https://doi.org/10.1175/2007MWR1978.1

Chadwick, C., 2021. Pseudo-nitzschia in the GOM, in: Gulf of Maine Stakeholders' Meeting.
Chapman, D.C., Beardsley, R.C., 1989. On the origin of shelf water in the Middle Atlantic Bight. J. Phys. Oceanogr. 19, 1–8.
Chen, Z., Kwon, Y.O., Chen, K., Fratantoni, P., Gawarkiewicz, G., Joyce, T.M., 2020. Long-Term SST variability on the Northwest Atlantic continental shelf and slope. Geophys. Res. Lett. 47, 1–11. https://doi.org/10.1029/2019GL085455
Chin, T.M., Vazquez-Cuervo, J., Armstrong, E.M., 2017. A multi-scale high-resolution analysis of global sea surface temperature. Remote Sens. Environ. 200, 154–169. https://doi.org/10.1016/j.rse.2017.07.029
Clark, S., Hubbard, K.A., Anderson, D.M., McGillicuddy, D.J.J., Ralston, D.K., Townsend, D.W., 2019. Pseudo-nitzschia bloom dynamics in the Gulf of Maine : 2012 – 2016. Harmful Algae 88, 101656. https://doi.org/10.1016/j.hal.2019.101656
Clark, S., Hubbard, K.A., McGillicuddy, D.J., Ralston, D.K., Shankar, S., 2021. Investigating Pseudo-nitzschia australis introduction to the Gulf of Maine with observations and models. Cont. Shelf Res. 104493. https://doi.org/10.1016/j.csr.2021.104493
Collins, M., Knutti, R., Arblaster, J., Dufresne, J.-L., Ficheft, T., Friedlingstein, P., Gao, X., Gutowski, W., Johns, T., Krinner, G., Shongwe, M., Tebaldi, C., Weaver, A.J., Wehner, M., Allen, M., Andrews, T., Beyerle, U., Bitz, C., Bony, S., Booth, B., Brooks, H., Brovkin, V., Browne, O., Brutel-Vuilmet, C., Cane, M., Chadwick, R., Cook, E., Cook, K., Eby, M., Fasullo, J., Fischer, E., Forest, C., Forster, P., Good, P., Goosse, H., Gregory, J., Hegerl, G., Hezel, P., Hodges, K., Holland, M., Huber, M., Huybrechts, P., Joshi, M., Kharin, V., Kushnir, Y., Larence, D., Lee, R., Liddicoat, S., Lucas, C., Lucht, W., Marotzke, J., Massonnet, F., Matthews, H.D., Meinshausen, M., Morice, C., Otto, A., Patricola, C., Philippon-Berthier, G., Prabhat, Rahmstorf, S., Riley, W., Rogelj, J., Saenko, O., Seager, R., Sedlacek, J., Shaffrey, L., Shindell, D., Sillmann, J., Slater, A., Stevens, B., Stott, P., Webb, R., Zappa, G., Zickfeld, K., 2013. Long-term climate change: Projections, commitments and irreversibility, in: Long-Term Climate Change: Projections, Commitments and Irreversibility. pp. 1029–1136. https://doi.org/10.1017/CBO9781107415324.024
Csanady, G.T., Hamilton, P., 1988. Circulation of slopewater. Cont. Shelf Res. 8, 565–624. https://doi.org/10.1016/0278-4343(88)90068-4
Cusack, C., Mouriño, H., Moita, M.T., Silke, J., 2015. Modelling Pseudo-nitzschia events off southwest Ireland. J. Sea Res. 105, 30–41. https://doi.org/10.1016/j.seares.2015.06.012
Dai, A., Qian, T., Trenberth, K.E., Milliman, J.D., 2009. Changes in continental freshwater discharge from 1948 to 2004. Am. Meteorol. Soc. 22, 2773–2792. https://doi.org/10.1175/2008JCLI2592.1
Davidson, K., Fehling, J., 2006. Modelling the influence of silicon and phosphorus limitation on the growth and toxicity of Pseudo-nitzschia seriata. African J. Mar. Sci. 28, 357–360. https://doi.org/10.2989/18142320609504177
Doney, S.C., 2006. Plankton in a warmer world. Nature 444.
Drenkard, E.J., Stock, C., Ross, A.C., Dixon, K.W., Adcroft, A., Alexander, M., Balaji, V., Bograd, S.J., Butenschön, M., Cheng, W., Curchitser, E., Lorenzo, E. Di, Dussin, R., Haynie, A.C., Harrison, M., Hermann, A., Hollowed, A., Holsman, K., Holt, J., Jacox, M.G., Jang, C.J., Kearney, K.A., Muhling, B.A., Buil, M.P., Saba, V., Sandø, A.B., Tommasi, D., Wang, M., 2021. Next-generation regional ocean projections for living marine resource management

837 in a changing climate. ICES J. Mar. Sci. https://doi.org/10.1093/icesjms/fsab100
838 Dunne, J.P., John, J.G., Adcroft, A.J., Griffies, S.M., Hallberg, R.W., Shevliakova, E., Stouffer, R.J.,
839 Cooke, W., Dunne, K.A., Harrison, M.J., Krasting, J.P., Malyshev, S.L., Milly, P.C.D., Phillipps,
840 P.J., Sentman, L.T., Samuels, B.L., Spelman, M.J., Winton, M., Wittenberg, A.T., Zadeh, N.,
841 2012. GFDL's ESM2 global coupled climate-carbon earth system models. Part I: Physical
842 formulation and baseline simulation characteristics. J. Clim. 25, 6646–6665.
843 https://doi.org/10.1175/JCLI-D-11-00560.1
844 Dunne, J.P., John, J.G., Shevliakova, S., Stouffer, R.J., Krasting, J.P., Malyshev, S.L., Milly, P.C.D.,
845 Sentman, L.T., Adcroft, A.J., Cooke, W., Dunne, K.A., Griffies, S.M., Hallberg, R.W., Harrison,
846 M.J., Levy, H., Wittenberg, A.T., Phillips, P.J., Zadeh, N., 2013. GFDL's ESM2 global coupled
847 climate-carbon earth system models. Part II: Carbon system formulation and baseline
848 simulation characteristics. J. Clim. 26, 2247–2267. https://doi.org/10.1175/JCLI-D-12-
849 00150.1
850 Fehling, J., Davidson, K., Bolch, C., Tett, P., 2006. Seasonality of Pseudo-nitzschia
851 spp.(Bacillariophyceae) in western Scottish waters. Mar. Ecol. Prog. Ser. 323, 91–105.
852 Fehling, J., Davidson, K., Bolch, C.J., Bates, S.S., 2004a. Growth and domoic acid production by
853 Pseudo-nitzschia seriata (Bacillariophyceae) under phosphate and silicate limitation. J.
854 Phycol. 40, 674–683. https://doi.org/10.1111/j.1529-8817.2004.03213.x
855 Fehling, J., Green, D.H., Davidson, K., Botch, C.J., Bates, S.S., 2004b. Domoic acid production by
856 Pseudo-nitzschia seriata (bacillariophyceae) in Scottish waters. J. Phycol. 40, 622–630.
857 https://doi.org/10.1111/j.1529-8817.2004.03200.x
858 Fernandes, L.F., Hubbard, K.A., Richlen, M.L., Smith, J., Bates, S.S., Ehrman, J., Léger, C., Mafra,
859 L.L., Kulis, D., Quilliam, M., Libera, K., McCauley, L., Anderson, D.M., 2014. Diversity and
860 toxicity of the diatom Pseudo-nitzschia Peragallo in the Gulf of Maine, Northwestern
861 Atlantic Ocean. Deep. Res. Part II Top. Stud. Oceanogr. 103, 139–162.
862 https://doi.org/10.1016/j.dsr2.2013.06.022
863 Fuentes, M.S., Wikfors, G.H., 2013. Control of domoic acid toxin expression in Pseudo-nitzschia
864 multiseries by copper and silica: Relevance to mussel aquaculture in New England (USA).
865 Mar. Environ. Res. 83, 23–28. https://doi.org/10.1016/j.marenvres.2012.10.005
866 Gobler, C.J., Doherty, O.M., Hattenrath-Lehmann, T.K., Griffith, A.W., Kang, Y., Litaker, R.W.,
867 2017. Ocean warming since 1982 has expanded the niche of toxic algal blooms in the
868 North Atlantic and North Pacific oceans. Proc. Natl. Acad. Sci. 114, 4975–4980.
869 https://doi.org/10.1073/pnas.1619575114
870 Gosling, S.N., Taylor, R.G., Arnell, N.W., Todd, M.C., 2011. A comparative analysis of projected
871 impacts of climate change on river runoff from global and catchment-scale hydrological
872 models. Hydrol. Earth Syst. Sci. 15, 279–294. https://doi.org/10.5194/hess-15-279-2011
873 Gosling, S.N., Zaherpour, J., Mount, N.J., Hattermann, F.F., Dankers, R., Arheimer, B., Breuer, L.,
874 Ding, J., Haddeland, I., Kumar, R., Kundu, D., Liu, J., van Griensven, A., Veldkamp, T.I.E.,
875 Vetter, T., Wang, X., Zhang, X., 2017. A comparison of changes in river runoff from multiple
876 global and catchment-scale hydrological models under global warming scenarios of 1 °C, 2
877 °C and 3 °C. Clim. Change 141, 577–595. https://doi.org/10.1007/s10584-016-1773-3
878 Haine, T.W.N., Curry, B., Gerdes, R., Hansen, E., Karcher, M., Lee, C., Rudels, B., Spreen, G., de
879 Steur, L., Stewart, K.D., Woodgate, R., 2015. Arctic freshwater export: Status, mechanisms,
880 and prospects. Glob. Planet. Change 125, 13–35.

https://doi.org/10.1016/j.gloplacha.2014.11.013
Hallegraeff, G.M., 2010. Ocean climate change, phytoplankton community responses, and harmful algal blooms: A formidable predictive challenge. J. Phycol. 46, 220–235. https://doi.org/10.1111/j.1529-8817.2010.00815.x
Han, G., Ma, Z., Long, Z., Perrie, W., Chassé, J., 2019. Climate Change on Newfoundland and Labrador Shelves: Results from a regional downscaled ocean and sea-ice model under an A1B forcing scenario 2011–2069. Atmos. - Ocean 57, 3–17. https://doi.org/10.1080/07055900.2017.1417110
Hardardóttir, S., Pančić, M., Tammilehto, A., Krock, B., Møller, E.F., Nielsen, T.G., Lundholm, N., 2015. Dangerous relations in the arctic marine food web: Interactions between toxin producing Pseudo-nitzschia diatoms and Calanus copepodites. Mar. Drugs 13, 3809–3835. https://doi.org/10.3390/md13063809
Hasle, G.R., 2002. Are most of the domoic acid-producing species of the diatom genus Pseudo-nitzschia cosmopolites? Harmful Algae 1, 137–146. https://doi.org/10.1016/S1568-9883(02)00014-8
He, R., McGillicuddy, D.J., 2008. Historic 2005 toxic bloom of Alexandrium fundyense in the west Gulf of Maine: 1. In situ observations of coastal hydrography and circulation. J. Geophys. Res. Ocean. 113, 1–12. https://doi.org/10.1029/2007JC004601
He, R., McGillicuddy, D.J., Keafer, B.A., Anderson, D.M., 2008. Historic 2005 toxic bloom of Alexandrium fundyense in the western Gulf of Maine: 2. Coupled biophysical numerical modeling. J. Geophys. Res. Ocean. 113, 1–12. https://doi.org/10.1029/2007JC004602
Hebert, D., Pettipas, R., Brickman, D., Dever, M., 2018. Meteorological, sea ice and physical oceanographic conditions on the Scotian Shelf and in the Gulf of Maine during 2016.
Hinder, S.L., Hays, G.C., Edwards, M., Roberts, E.C., Walne, A.W., Gravenor, M.B., 2012. Changes in marine dinoflagellate and diatom abundance under climate change. Nat. Clim. Chang. 2, 271–275. https://doi.org/10.1038/nclimate1388
IPCC, Pachauri, R.K., Meyer, L.A., 2014. Climate Change 2014: Synthesis Report. Contribution of Working Groups I, II and III to the Fifth Assessment Report of the Intergovernmental Panel on Climate Change. Geneva, Switzerland.
John, J.G., Stock, C.A., Dunne, J.P., 2015. A more productive, but different, ocean after mitigation. Geophys. Res. Lett. 42, 9836–9845. https://doi.org/10.1002/2015GL066160
Kang, D., Curchitser, E.N., 2013. Gulf Stream eddy characteristics in a high-resolution ocean model. J. Geophys. Res. Ocean. 118, 4474–4487. https://doi.org/10.1002/jgrc.20318
Keafer, B.A., Churchill, J.H., McGillicuddy, D.J., Anderson, D.M., 2005. Bloom development and transport of toxic Alexandrium fundyense populations within a coastal plume in the Gulf of Maine. Deep. Res. Part II Top. Stud. Oceanogr. 52, 2674–2697. https://doi.org/10.1016/j.dsr2.2005.06.016
Knutson, T.R., Zeng, F., 2018. Model assessment of observed precipitation trends over land regions: Detectable human influences and possible low bias in model trends. J. Clim. 31, 4617–4637. https://doi.org/10.1175/JCLI-D-17-0672.1
Knutti, R., Sedláček, J., 2013. Robustness and uncertainties in the new CMIP5 climate model projections. Nat. Clim. Chang. 3, 369–373. https://doi.org/10.1038/nclimate1716
Large, W.G., Yeager, S.G., 2009. The global climatology of an interannually varying air - sea flux data set. Clim. Dyn. 33, 341–364. https://doi.org/10.1007/s00382-008-0441-3

925 Lema, K.A., Latimier, M., Nézan, É., Fauchot, J., Le Gac, M., 2017. Inter and intra-specific growth
926 and domoic acid production in relation to nutrient ratios and concentrations in Pseudo-
927 nitzschia: phosphate an important factor. Harmful Algae 64, 11–19.
928 https://doi.org/10.1016/j.hal.2017.03.001
929 Li, Y., He, R., Chen, K., McGillicuddy, D.J., 2015. Variational data assimilative modeling of the
930 Gulf of Maine in spring and summer 2010. J. Geophys. Res. Ocean. 132, 1–17.
931 https://doi.org/10.1002/2014JC010320.Received
932 Li, Y., He, R., McGillicuddy, D.J., 2014. Seasonal and interannual variability in Gulf of Maine
933 hydrodynamics: 2002-2011. Deep. Res. Part II Top. Stud. Oceanogr. 103, 210–222.
934 https://doi.org/10.1016/j.dsr2.2013.03.001
935 Li, Y., He, R., McGillicuddy, D.J., Anderson, D.M., Keafer, B.A., 2009. Investigation of the 2006
936 Alexandrium fundyense bloom in the Gulf of Maine: In-situ observations and numerical
937 modeling. Cont. Shelf Res. 29, 2069–2082. https://doi.org/10.1016/j.csr.2009.07.012
938 Li, Y., Stumpf, R.P., McGillicuddy, D.J., He, R., 2020. Dynamics of an intense Alexandrium
939 catenella red tide in the Gulf of Maine: satellite observations and numerical modeling.
940 Harmful Algae 99, 101927. https://doi.org/10.1016/j.hal.2020.101927
941 Loder, J.W., Petrie, B., Gawarkiewicz, G., 1998. The coastal ocean off northwestern North
942 America: a large-scale view., in: The Sea, Vol 11. pp. 105–133.
943 Luerssen, R.M., Thomas, A.C., Hurst, J., 2005. Relationships between satellite-measured thermal
944 features and Alexandrium-imposed toxicity in the Gulf of Maine. Deep. Res. Part II Top.
945 Stud. Oceanogr. 52, 2656–2673. https://doi.org/10.1016/j.dsr2.2005.06.025
946 Lundholm, N., Clarke, A., Ellegaard, M., 2010. A 100-year record of changing Pseudo-nitzschia
947 species in a sill-fjord in Denmark related to nitrogen loading and temperature. Harmful
948 Algae 9, 449–457. https://doi.org/10.1016/j.hal.2010.03.001
949 Lundholm, N., Hansen, P.J., Kotaki, Y., 2004. Effect of pH on growth and domoic acid production
950 by potentially toxic diatoms of the genera Pseudo-nitzschia and Nitzschia. Mar. Ecol. Prog.
951 Ser. 273, 1–15. https://doi.org/10.3354/meps273001
952 Lundholm, N., Krock, B., John, U., Skov, J., Cheng, J., Pančić, M., Wohlrab, S., Rigby, K., Nielsen,
953 T.G., Selander, E., Harðardóttir, S., 2018. Induction of domoic acid production in diatoms—
954 Types of grazers and diatoms are important. Harmful Algae.
955 https://doi.org/10.1016/j.hal.2018.06.005
956 Lynch, D.R., Holboke, M.J., Naimie, C.E., 1997. The Maine coastal current: Spring climatological
957 circulation. Cont. Shelf Res. 17, 605–634. https://doi.org/10.1016/S0278-4343(96)00055-6
958 Maldonado, M.T., Hughes, M.P., Rue, E.L., Wells, M.L., 2002. The effect of Fe and Cu on growth
959 and domoic acid production by Pseudo-nitzschia multiseries and Pseudo-nitzschia
960 australis. Limnol. Oceanogr. 47, 515–526. https://doi.org/10.4319/lo.2002.47.2.0515
961 Marchetti, A., Trainer, V.L., Harrison, P.J., 2004. Environmental conditions and phytoplankton
962 dynamics associated with Pseudo-nitzschia abundance and domoic acid in the Juan de
963 Fuca eddy. Mar. Ecol. Prog. Ser. 281, 1–12. https://doi.org/10.3354/meps281001
964 McCabe, R.M., Hickey, B.M., Kudela, R.M., Lefebvre, K.A., Adams, N.G., Bill, B.D., Gulland,
965 F.M.D., Thomson, R.E., Cochlan, W.P., Trainer, V.L., 2016. An unprecedented coastwide
966 toxic algal bloom linked to anomalous ocean conditions. Geophys. Res. Lett. 43, 10,366-
967 10,376. https://doi.org/10.1002/2016GL070023
968 McGillicuddy, D. J., Townsend, D.W., He, R., Keafer, B.A., Kleindinst, J.L., Li, Y., Manning, J.P.,

969 Mountain, D.G., Thomas, M.A., Anderson, D.M., 2011. Suppression of the 2010
970 Alexandrium fundyense bloom by changes in physical, biological, and chemical properties
971 of the Gulf of Maine. Limnol. Oceanogr. 56, 2411–2426.
972 https://doi.org/10.4319/lo.2011.56.6.2411
973 McGillicuddy, D J, Townsend, D.W., He, R., Keafer, B.A., Kleindinst, J.L., Li, Y., Manning, J.P.,
974 Mountain, D.G., Thomas, M.A., Anderson, D.M., 2011. Suppression of the 2010
975 Alexandrium fundyense bloom by changes in physical, biological, and chemical properties
976 of the Gulf of Maine. Limnol. Oceanogr. 56, 2411–2426.
977 https://doi.org/10.4319/lo.2011.56.6.2411
978 McGillicuddy, D.J., Townsend, D.W., Keafer, B.A., Thomas, M.A., Anderson, D.M., 2014. Georges
979 Bank: A leaky incubator of Alexandrium fundyense blooms. Deep. Res. Part II Top. Stud.
980 Oceanogr. 103, 163–173. https://doi.org/10.1016/j.dsr2.2012.11.002
981 McKibben, S.M., Peterson, W., Wood, A.M., Trainer, V.L., Hunter, M., White, A.E., 2017. Climatic
982 regulation of the neurotoxin domoic acid. Proc. Natl. Acad. Sci. 114, 239–244.
983 https://doi.org/10.1073/pnas.1606798114
984 Mesinger, F., DiMego, G., Kalnay, E., Mitchell, K., 2006. North American Regional Reanalysis.
985 Bull. Am. Meteorol. Soc. 87, 343–360. https://doi.org/10.1175/BAMS-87-3-343
986 Miller, C.B., Wheeler, P.A., 2012. Biological Oceanography.
987 Moore, S.K., Dreyer, S.J., Ekstrom, J.A., Moore, K., Norman, K., Klinger, T., Allison, E.H., Jardine,
988 S.L., 2020. Harmful algal blooms and coastal communities: Socioeconomic impacts and
989 actions taken to cope with the 2015 U.S. West Coast domoic acid event. Harmful Algae 96,
990 101799. https://doi.org/10.1016/j.hal.2020.101799
991 Moore, S.K., Mantua, N.J., Salathé, E.P., 2011. Past trends and future scenarios for
992 environmental conditions favoring the accumulation of paralytic shellfish toxins in Puget
993 Sound shellfish. Harmful Algae 10, 521–529. https://doi.org/10.1016/j.hal.2011.04.004
994 Moore, S.K., Trainer, V.L., Mantua, N.J., Parker, M.S., Laws, E.A., Backer, L.C., Fleming, L.E.,
995 2008. Impacts of climate variability and future climate change on harmful algal blooms and
996 human health. Environ. Heal. 12, 1–12. https://doi.org/10.1186/1476-069X-7-S2-S4
997 Palmer, M.C., Deroba, J.J., Legault, C.M., Brooks, E.N., 2016. Comment on “Slow adaptation in
998 the face of rapid warming leads to collapse of the Gulf of Maine cod fishery.” Science (80-.
999). 352, 423. https://doi.org/10.1126/science.aae0463
1000 Park, J.M., Archer, S.D., Hubbard, K.A., Poulton, N., Countway, P.D., 2018. Effects of phosphate
1001 limitation on cell growth and toxin production in Pseudo-nitzschia in the Gulf of Maine, in:
1002 Oral Presentation at the AGU Ocean Sciences Meeting. American Geophysical Union,
1003 Portland, Oregon.
1004 Parsons, M.L., Dortch, Q., Turner, R.E., 2002. Sedimentological evidence of an increase in
1005 Pseudo-nitzschia (Bacillariophyceae) abundance in response to coastal eutrophication.
1006 Limnol. Oceanogr. 47, 551–558. https://doi.org/10.4319/lo.2002.47.2.0551
1007 Pershing, A.J., Alexander, M.A., Hernandez, C.M., Kerr, L.A., Bris, A. Le, Mills, K.E., Nye, J.A.,
1008 Record, N.R., Scannell, H.A., Scott, J.D., Sherwood, G.D., Thomas, A.C., 2016. Response to
1009 comments on "Slow adaptation in the face of rapid warming leads to collapse of the Gulf
1010 of Maine cod fishery. Science (80-.). 352, 423. https://doi.org/10.1126/science.aae0463
1011 Pershing, A.J., Alexander, M.A., Hernandez, C.M., Kerr, L.A., Le Bris, A., Mills, K.E., Nye, J.A.,
1012 Record, N.R., Scannell, H.A., Scott, J.D., Sherwood, G.D., Thomas, A.C., 2015. Slow

adaptation in the face of rapid warming leads to collapse of the Gulf of Maine cod fishery. Science (80-.). 350, 809–812. https://doi.org/10.1126/science.aac9819
Pershing, A.J., Mills, K.E., Dayton, A.M., Franklin, B.S., Kennedy, B.T., 2018. Evidence for adaptation from the 2016 marine heatwave in the Northwest Atlantic Ocean. Oceanography 31. https://doi.org/https://doi.org/10.5670/oceanog.2018.213
Pettigrew, N.R., Churchill, J.H., Janzen, C.D., Mangum, L.J., Signell, R.P., Thomas, A.C., Townsend, D.W., Wallinga, J.P., Xue, H., 2005. The kinematic and hydrographic structure of the Gulf of Maine Coastal Current. Deep. Res. Part II Top. Stud. Oceanogr. 52, 2369–2391. https://doi.org/10.1016/j.dsr2.2005.06.033
Prudhomme, C., Davies, H., 2009. Assessing uncertainties in climate change impact analyses on the river flow regimes in the UK. Part 1: Baseline climate. Clim. Change 93, 177–195. https://doi.org/10.1007/s10584-008-9464-3
Ralston, D.K., Moore, S.K., 2020. Modeling harmful algal blooms in a changing climate. Harmful Algae 91, 101729. https://doi.org/10.1016/j.hal.2019.101729
Ryan, J.P., Kudela, R.M., Birch, J.M., Blum, M., Bowers, H.A., Chavez, F.P., Doucette, G.J., Hayashi, K., Marin, R., Mikulski, C.M., Pennington, J.T., Scholin, C.A., Smith, G.J., Woods, A., Zhang, Y., 2017. Causality of an extreme harmful algal bloom in Monterey Bay, California, during the 2014–2016 northeast Pacific warm anomaly. Geophys. Res. Lett. 44, 5571–5579. https://doi.org/10.1002/2017GL072637
Saba, V.S., Griffies, S.M., Anderson, W.G., Winton, M., Alexander, M.A., Delworth, T.L., Hare, J.A., Harrison, M.J., Rosati, A., Vecchi, G.A., Zhang, R., 2016. Enhanced warming of the Northwest Atlantic Ocean under climate change. J. Geophys. Res. Ocean. 121, 118–132. https://doi.org/10.1002/2015JC011346
Santiago-Morales, I.S., García-Mendoza, E., 2011. Growth and domoic acid content of Pseudo-nitzschia australis isolated from northwestern Baja California, Mexico, cultured under batch conditions at different temperatures and two Si:NO3 ratios. Harmful Algae 12, 82–94. https://doi.org/10.1016/j.hal.2011.09.004
Schnetzer, A., Jones, B.H., Schaffner, R.A., Cetinic, I., Fitzpatrick, E., Miller, P.E., Seubert, E.L., Caron, D.A., 2013. Coastal upwelling linked to toxic Pseudo-nitzschia australis blooms in Los Angeles coastal waters, 2005-2007. J. Plankton Res. 35, 1080–1092. https://doi.org/10.1093/plankt/fbt051
Schnetzer, A., Miller, P.E., Schaffner, R.A., Stauffer, B.A., Jones, B.H., Weisberg, S.B., DiGiacomo, P.M., Berelson, W.M., Caron, D.A., 2007. Blooms of Pseudo-nitzschia and domoic acid in the San Pedro Channel and Los Angeles harbor areas of the Southern California Bight, 2003-2004. Harmful Algae 6, 372–387. https://doi.org/10.1016/j.hal.2006.11.004
Seegers, B.N., Birch, J.M., Marin, R., Scholin, C.A., Caron, D.A., Seubert, E.L., Howard, M.D.A., Robertson, G.L., Jones, B.H., 2015. Subsurface seeding of surface harmful algal blooms observed through the integration of autonomous gliders, moored environmental sample processors, and satellite remote sensing in southern California. Limnol. Oceanogr. 60, 754–764. https://doi.org/10.1002/lno.10082
Shchepetkin, A.., McWilliams, J.C., 2005. The regional oceanic modeling system (ROMS): A split-explicit, free-surface, topography-following-coordinate oceanic model. Ocean Model. 9, 347–404.
Shchepetkin, A.F., McWilliams, J.C., 2003. A method for computing horizontal pressure-gradient

force in an oceanic model with a nonaligned vertical coordinate. J. Geophys. Res. 108, 3090.
Shin, S.-I., Alexander, M.A., 2020a. Dynamical downscaling of future hydrographic changes over the Northwest Atlantic Ocean. Am. Meteorol. Soc. 33, 2871–2890. https://doi.org/10.1175/JCLI-D-19-0483.1
Shin, S.-I., Alexander, M.A., 2020b. Dynamical downscaling of future hydrographic changes over the Northwest Atlantic Ocean. J. Clim. 33, 2871–2890. https://doi.org/10.1175/jcli-d-19-0483.1
Smith, R.E.H., Stapleford, L.C., Ridings, R.S., 1994. The acclimate response of growth, photosynthesis, composition, and carbon balance to temperature in the psychrophilic ice diatom Nitzschia seriata. J. Phycol. 30, 8–16. https://doi.org/https://doi.org/10.1111/j.0022-3646.1994.00008.x
Song, H., Ji, R., Stock, C., Kearney, K., Wang, Z., 2011. Interannual variability in phytoplankton blooms and plankton productivity over the Nova Scotian Shelf and in the Gulf of Maine. Mar. Ecol. Prog. Ser. 426, 105–118. https://doi.org/10.3354/meps09002
Sverdrup, H.U., 1953. On conditions for the vernal bloom of phytoplankton. J.Cons.Perm.Int.Explor.Mer 18, 287–295.
Tammilehto, A., Nielsen, T.G., Krock, B., Møller, E.F., Lundholm, N., 2015. Induction of domoic acid production in the toxic diatom Pseudo-nitzschia seriata by calanoid copepods. Aquat. Toxicol. 159, 52–61. https://doi.org/10.1016/j.aquatox.2014.11.026
Tatters, A.O., Fu, F.X., Hutchins, D.A., 2012. High CO 2 and silicate limitation synergistically increase the toxicity of Pseudo-nitzschia fraudulenta. PLoS One 7. https://doi.org/10.1371/journal.pone.0032116
Terseleer, N., Gypens, N., Lancelot, C., 2013. Factors controlling the production of domoic acid by Pseudo-nitzschia (Bacillariophyceae): A model study. Harmful Algae 24, 45–53. https://doi.org/10.1016/j.hal.2013.01.004
Thessen, A.E., Stoecker, D.K., 2008. Distribution, abundance and domoic acid analysis of the toxic diatom genus Pseudo-nitzschia from the Chesapeake Bay. Estuaries and Coasts 31, 664–672. https://doi.org/10.1007/s12237-008-9053-8
Thomas, A.C., Pershing, A.J., Friedland, K.D., Nye, J.A., Mills, K.E., Alexander, M.A., Record, N.R., Weatherbee, R., Elisabeth Henderson, M., 2017a. Seasonal trends and phenology shifts in sea surface temperature on the North American northeastern continental shelf. Elementa 5. https://doi.org/10.1525/elementa.240
Thomas, A.C., Pershing, A.J., Friedland, K.D., Nye, J.A., Mills, K.E., Alexander, M.A., Record, N.R., Weatherbee, R., Elisabeth Henderson, M., 2017b. Seasonal trends and phenology shifts in sea surface temperature on the North American northeastern continental shelf. Elementa 5, 1–17. https://doi.org/10.1525/elementa.240
Thomas, M.K., Kremer, C.T., Klausmeier, C.A., Litchman, E., 2012. A global pattern of thermal adaptation in marine phytoplankton. Science (80-.). 338, 1085–1088. https://doi.org/10.1126/science.1224836
Thorel, M., Fauchot, J., Morelle, J., Raimbault, V., Le Roy, B., Miossec, C., Kientz-Bouchart, V., Claquin, P., 2014. Interactive effects of irradiance and temperature on growth and domoic acid production of the toxic diatom Pseudo-nitzschia australis (Bacillariophyceae). Harmful Algae 39, 232–241. https://doi.org/10.1016/j.hal.2014.07.010

Townsend, D.W., McGillicuddy, D.J., Thomas, M.A., Rebuck, N.D., 2014. Nutrients and water masses in the Gulf of Maine-Georges Bank region: Variability and importance to blooms of the toxic dinoflagellate Alexandrium fundyense. Deep. Res. Part II Top. Stud. Oceanogr. 103, 238–263. https://doi.org/10.1016/j.dsr2.2013.08.003

Townsend, D.W., Pettigrew, N.R., Thomas, A.C., 2001. Offshore blooms of the red tide dinoflagellate, Alexandrium sp., in the Gulf of Maine. Cont. Shelf Res. 21, 347–369. https://doi.org/10.1016/S0278-4343(00)00093-5

Townsend, D.W., Pettigrew, N.R., Thomas, M.A., Neary, M.G., Mcgillicuddy, D.J., Donnell, J.O., 2015. Water masses and nutrient sources to the Gulf of Maine. J. Mar. Res. 141, 93–122. https://doi.org/10.1038/141548c0

Townsend, D.W., Rebuck, N.D., Thomas, M.A., Karp-Boss, L., Gettings, R.M., 2010. A changing nutrient regime in the Gulf of Maine. Cont. Shelf Res. 30, 820–832. https://doi.org/10.1016/j.csr.2010.01.019

Townsend, D.W., Thomas, A.C., Mayer, L.M., Thomas, M.A., Quinlan, J.A., 2006. Oceanography of the Northwest Atlantic Shelf (1, W), in: The Sea: The Global Coastal Ocean: Interdisciplinary Regional Studies and Syntheses. Harvard University Press, pp. 119–168.

Trainer, V.L., Adams, N.G., Bill, B.D., Stehr, C.M., Wekell, J.C., Moeller, P., Busman, M., Woodruff, D., 2000. Domoic acid production near California coastal upwelling zones, June 1998. Limnol. Oceanogr. 45, 1818–1833. https://doi.org/10.4319/lo.2000.45.8.1818

Trainer, V.L., Moore, S.K., Hallegraeff, G., Kudela, R.M., Clement, A., Mardones, J.I., Cochlan, W.P., 2020. Pelagic harmful algal blooms and climate change: Lessons from nature's experiments with extremes. Harmful Algae 91, 101591. https://doi.org/10.1016/j.hal.2019.03.009

USGS, 2013. Water Data for the Nation [WWW Document]. URL https://waterdata.usgs.gov/nwis

Vavrus, S.J., Holland, M.M., Jahn, A., Bailey, D.A., Blazey, B.A., 2012. Twenty-first-century arctic climate change in CCSM4. J. Clim. 25, 2696–2710. https://doi.org/10.1175/JCLI-D-11-00220.1

Wells, M.L., Karlson, B., Wulff, A., Kudela, R., Trick, C., Asnaghi, V., Berdalet, E., Cochlan, W., Davidson, K., De Rijcke, M., Dutkiewicz, S., Hallegraeff, G., Flynn, K.J., Legrand, C., Paerl, H., Silke, J., Suikkanen, S., Thompson, P., Trainer, V.L., 2020. Future HAB science: Directions and challenges in a changing climate. Harmful Algae 91. https://doi.org/10.1016/j.hal.2019.101632

Xue, H., Chai, F., Pettigrew, N.R., 2000. A model study of the seasonal circulation in the Gulf of Maine. J. Phys. Oceanogr. 30, 1111–1135. https://doi.org/10.1175/1520-0485(2000)030<1111:AMSOTS>2.0.CO;2

Zhu, Z., Qu, P., Fu, F., Tennenbaum, N., Tatters, A.O., Hutchins, D.A., 2017. Understanding the blob bloom: Warming increases toxicity and abundance of the harmful bloom diatom Pseudo-nitzschia in California coastal waters. Harmful Algae 67, 36–43. https://doi.org/10.1016/j.hal.2017.06.004

7 Supplementary Material

7.1 Additional Information Regarding the Delta Method and Boundary Conditions

Delta method sources and application:

Table S-3 - Model fields to which Deltas were added, and the source from which Deltas were calculated. Note that ROMS can read humidity as either relative humidity (%) or specific humidity (g kg^{-1})

Description	ROMS Variable	Units	Source
3D salinity	salt	PSU	NWA ROMS output
3D temperature	temp	°C	
3D velocity	u/v	m/s	
2D sea surface height	zeta	m	
Sea level air pressure	P_{air}	mbar	GFDL-ESM2M
Surface relative humidity	Q_{air}	%	
Surface air temperature	T_{air}	°C	
10m wind velocity	u_{wind} /v_{wind}	m s^{-1}	
Rainfall rate	rain	kg (m^{-2} s^{-1})	
Downwelling longwave radiation	lwrad	$W\ m^{-2}$	
Downwelling shortwave radiation	swrad	$W\ m^{-2}$	
River runoff	River transport	m^3 s^{-1}	GFDL-ESM2M

GOM ROMS Boundary Conditions:

Variable	**Boundary Type**
Free-surface (eta)	Chapman implicit
2-D (depth-averaged) velocity (u/v)	Flather
3-D velocity (u/v)	Radiation
Temperature/Salinity	Radiation-Nudging

More details about how the Delta Method was implemented:

1. Monthly Deltas were calculated from the variables on the NWA ROMS grid.
2. The result from step 1 was interpolated from the NWA ROMS grid to the GOM ROMS grid with the Rutgers toolbox function, roms2roms.m (This uses the Matlab function TriScatteredInterp, which in turn uses a Delaunay triangulation of the variable to generate a function that goes through the input points and can be queried at any 3-D point.)
3. The interpolated Delta value was extracted at the correct indices for each boundary. Depth-integrated velocities were calculated at all grid cells and then extracted at the boundaries.
4. The result of #3 was added to the hindcast boundary conditions.
5. The model was re-run with the same setup as the hindcast but with the new initial and boundary conditions.

7.2 Results

In the projection the inflow ratio increased by 0.1 on average, or 20% of the hindcast ratio.

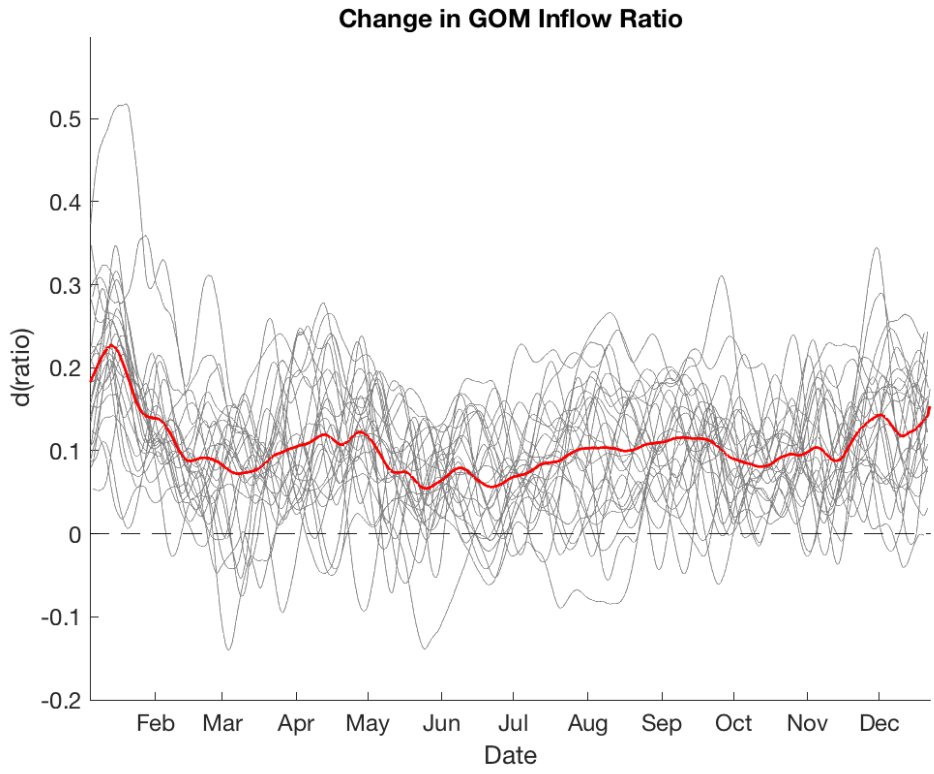

Figure S-1 – Change in GOM inflow ratio vs. day of the year. The differences between individual projections and hindcasts for each year are plotted in grey. The difference between the projected composite year and the hindcast composite year is plotted in red. Data were smoothed over a weekly time scale before plotting.

Both models projected an increase in the GOM inflow ratio.

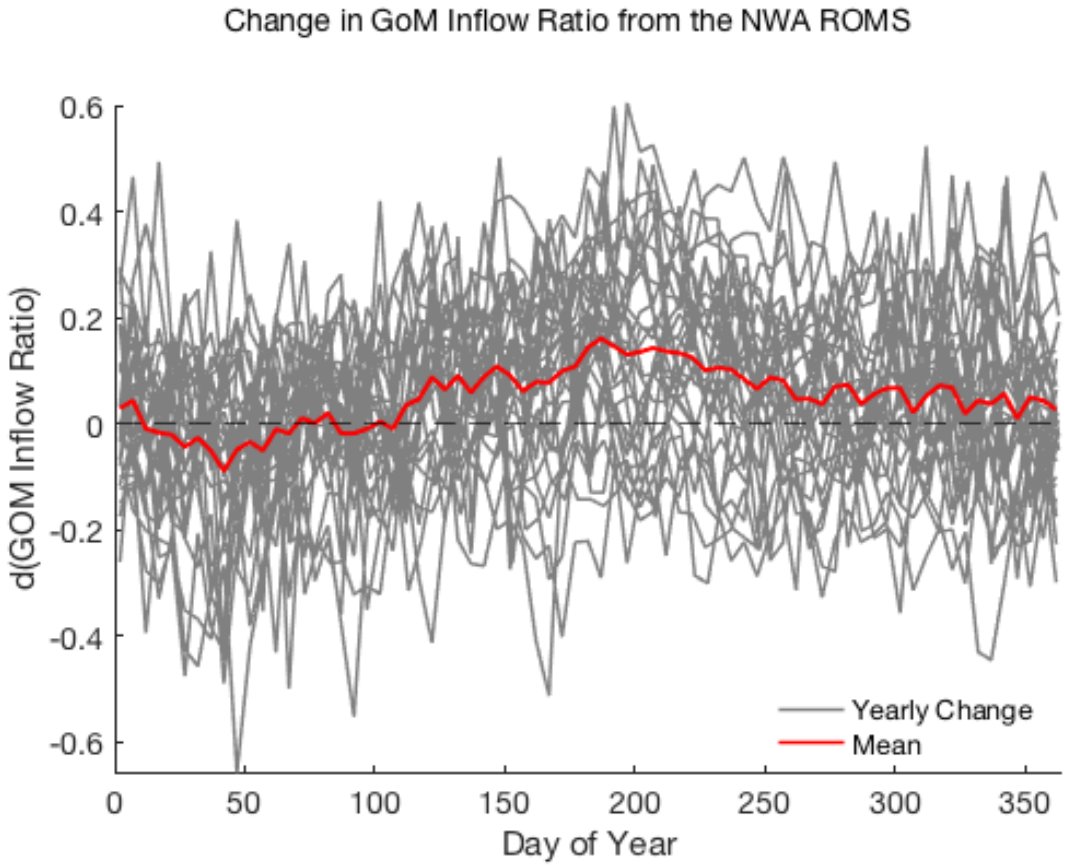

Figure S-2 - Change in the GOM inflow ratio vs. day of the year as calculated from NWA ROMS output. The differences between individual projections and hindcasts for each year are plotted in grey. The difference between the projected composite year and the hindcast composite year is plotted in red. The ratio was calculated and plotted at the 3-day output resolution of the NWA ROMS.

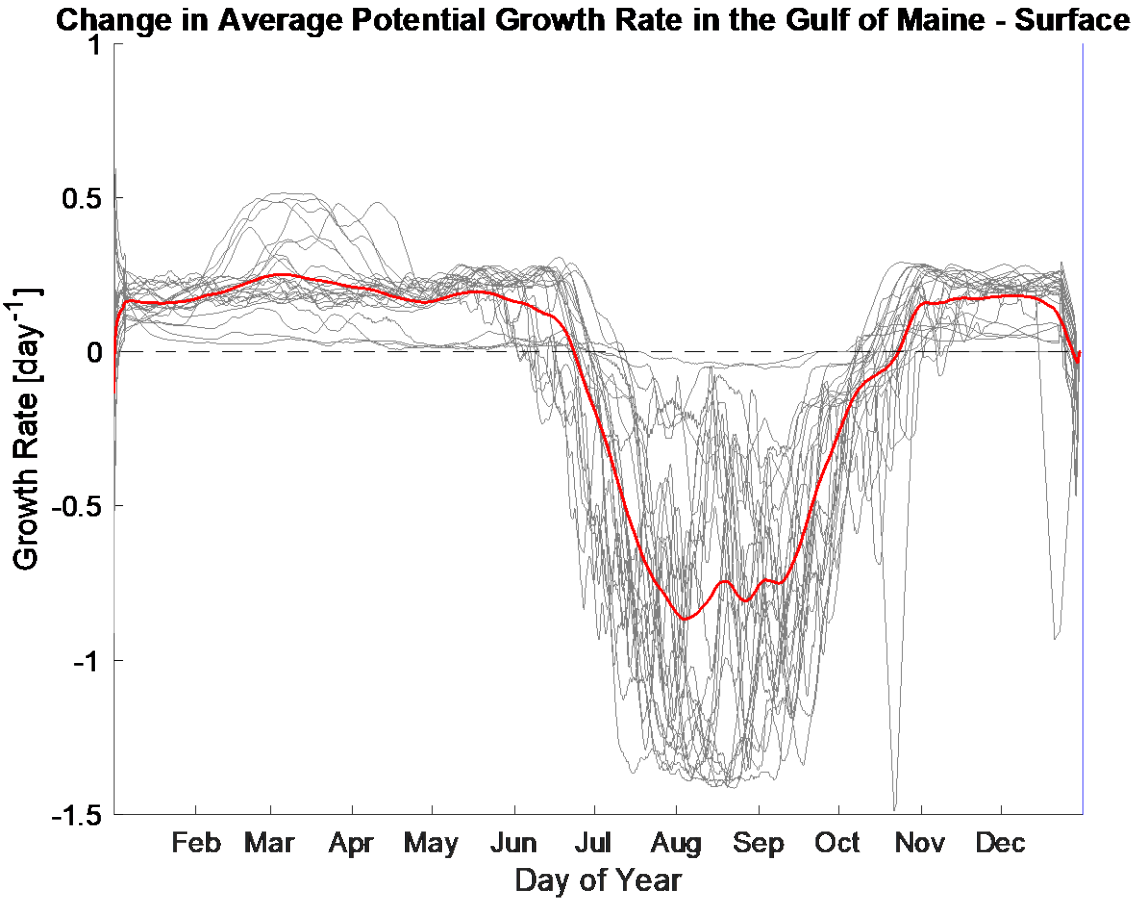

Figure S-3 – Change in P. australis *potential growth at the surface vs. day of the year. The differences between individual projections and hindcasts for each year are plotted in grey. The difference between the projected composite year and the hindcast composite year is plotted in red. Data were averaged over the Gulf of Maine before plotting.*

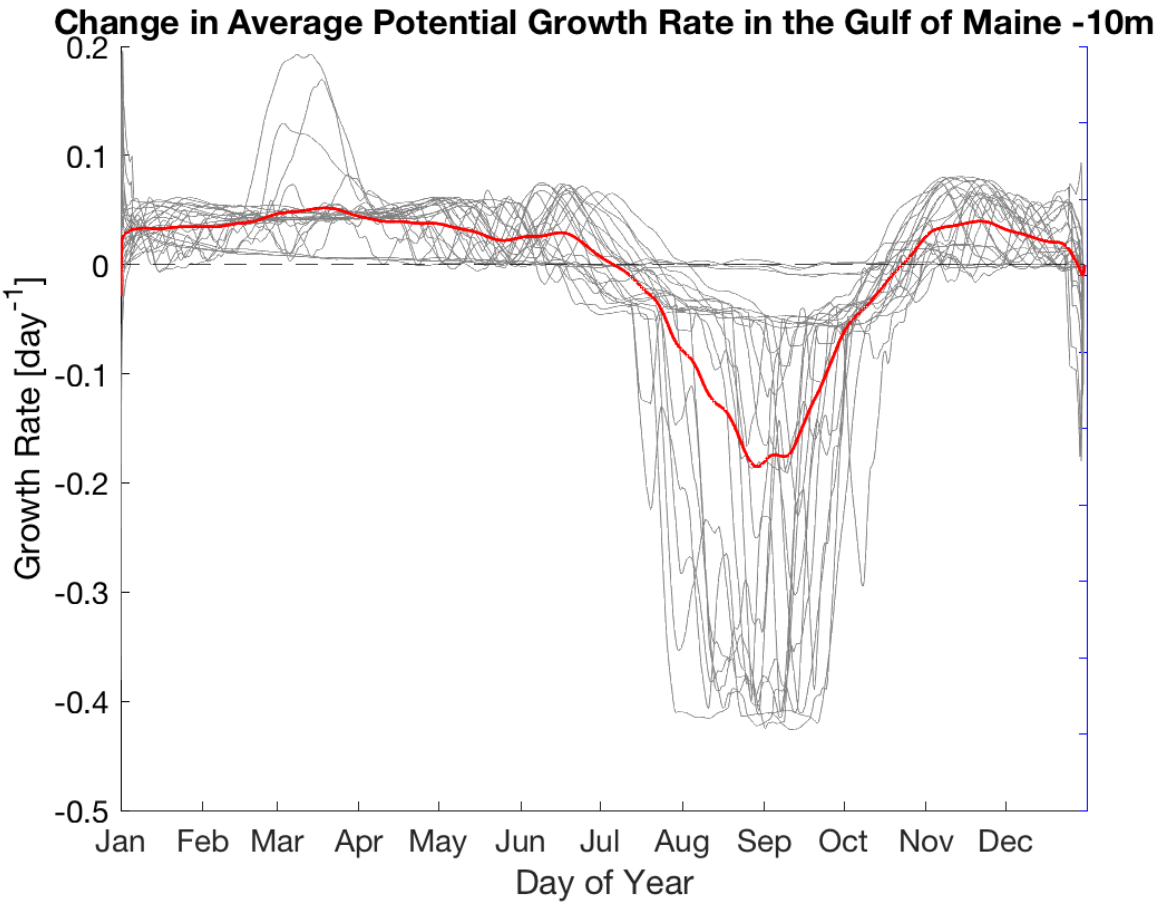

Figure S-4 - Change in P. australis *potential growth at the surface vs. day of the year. The differences between individual projections and hindcasts for each year are plotted in grey. The difference between the projected composite year and the hindcast composite year is plotted in red. Data were averaged over the Gulf of Maine before plotting*

7.3 Discussion

Surface salinity decreased by 0.3 PSU on average in the NWA ROMS projection within the GOM ROMS domain, but by 0.9 PSU on average in the GOM ROMS projection.

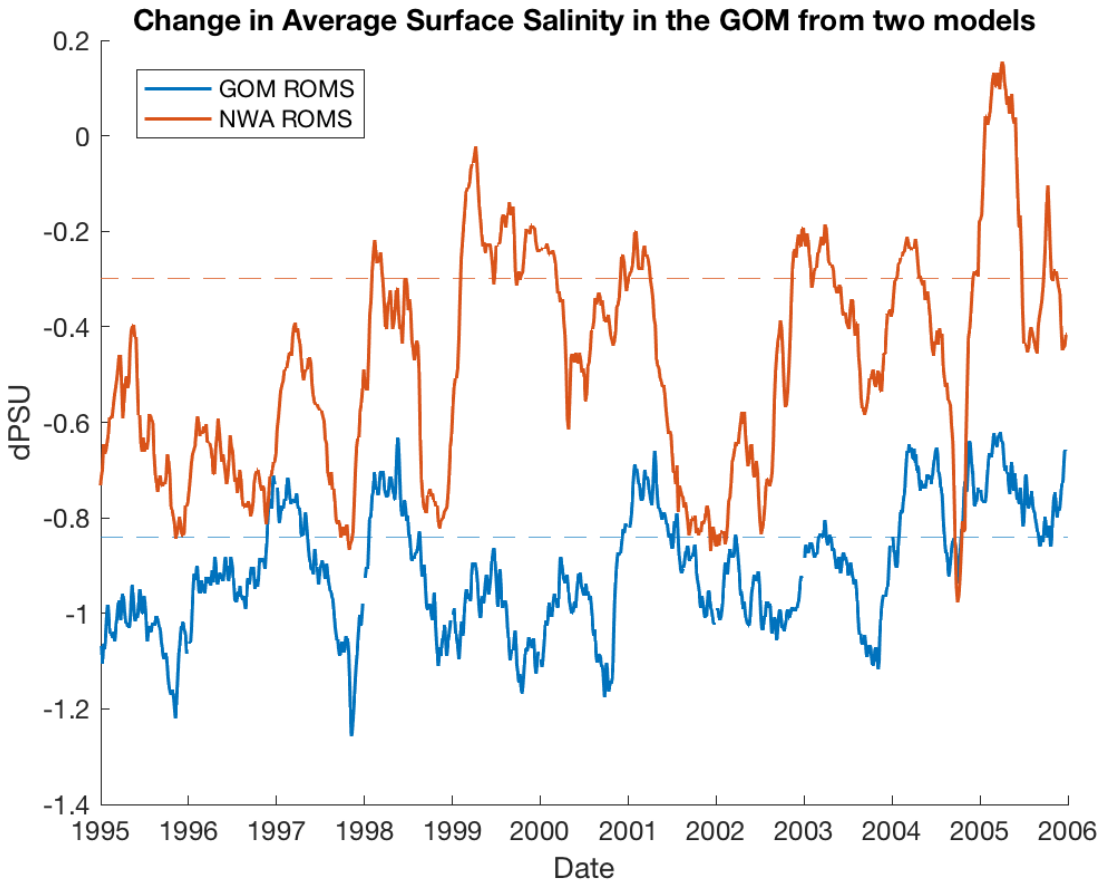

Figure S-5 - Change in average surface salinity in the GOM ROMS domain vs. time from (blue) the GOM ROMS and (red) the NWA ROMS. NWA ROMS data were interpolated to the GOM ROMS grid before plotting. Data are only plotted for the time period when the two model simulations overlap.

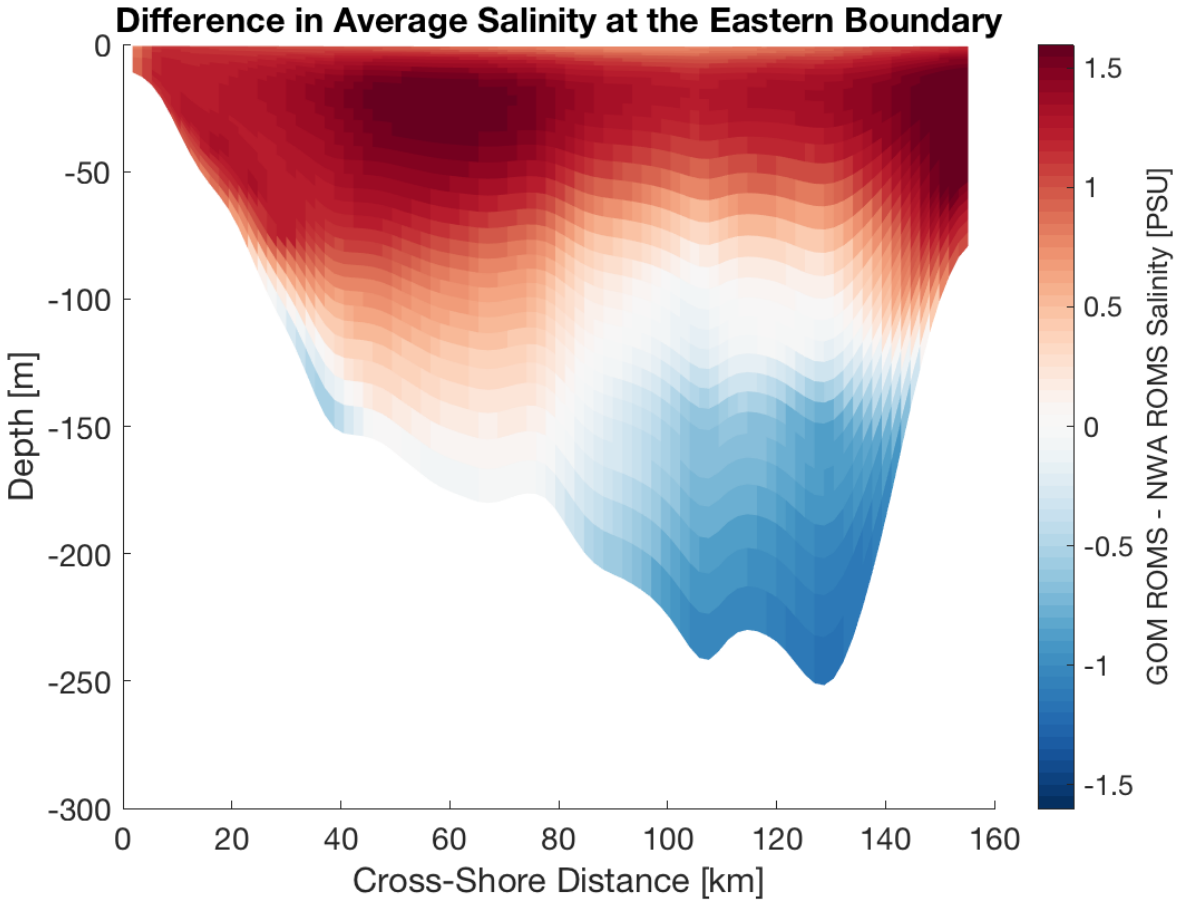

Figure S-6 - Contours of the difference in average salinity between the GOM ROMS and the NWA ROMS at the GOM ROMS eastern boundary. Depth in meters is shown on the y axis, and cross-shore distance in km is shown on the x axis, with the coastline to the left. Corresponding color values are given in the color bars on the right.

In the projected composite year, while the average surface temperature in most of the domain was 16°C, this water mass remained between 8 and 12°C.

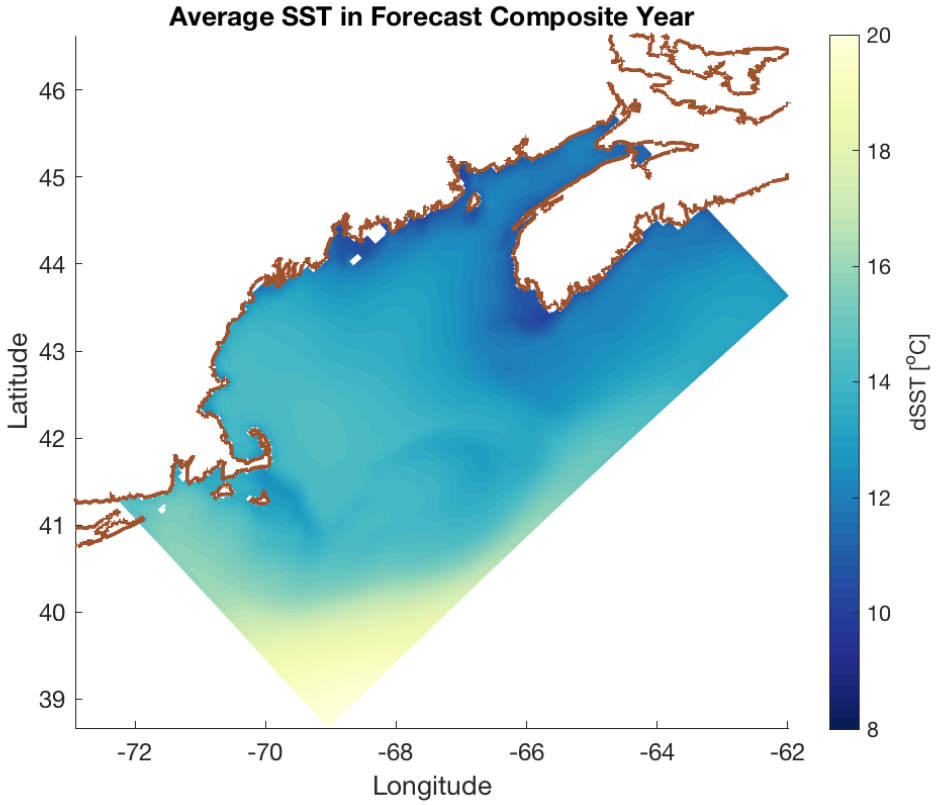

Figure S-7 - Average SST in the projected composite year. Color scale is defined by the color bar on the right.

To assess how these species' growth might change as a result of warming temperatures, the *P. australis* growth curve was shifted to their corresponding temperature ranges such that the curve approached zero at 15°C for *P. seriata* and growth peaked at 17°C for *P. plurisecta.*

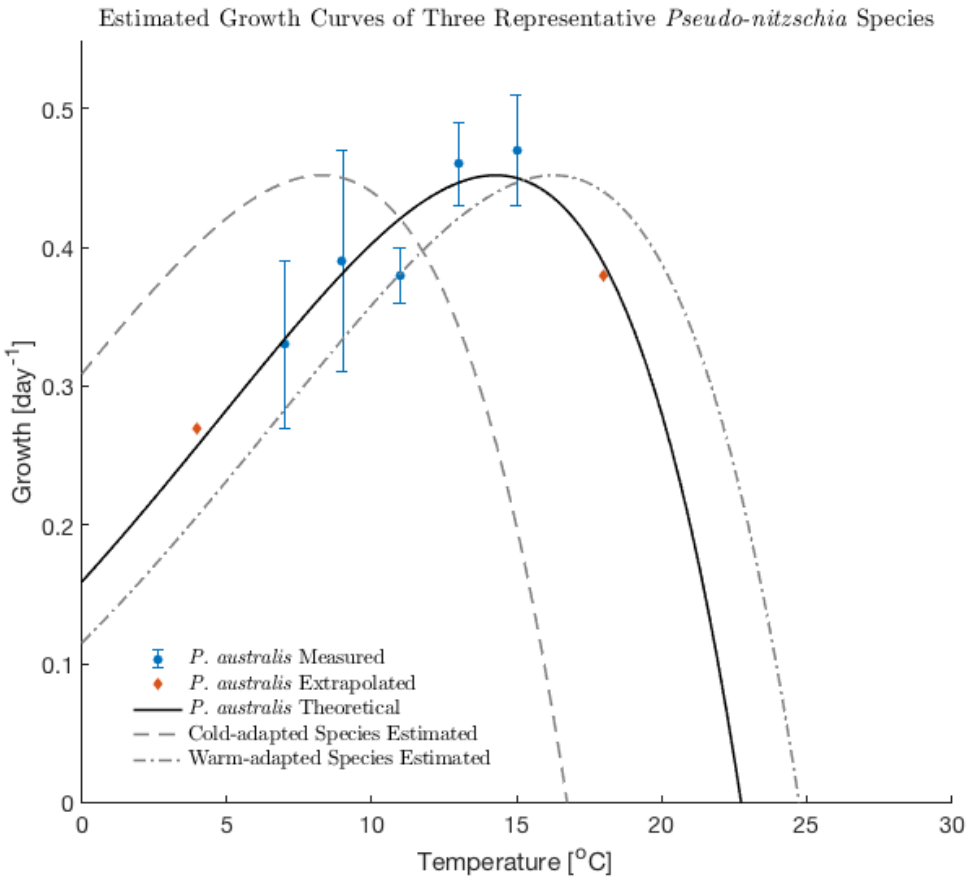

Figure S-8 – Same as Figure 3, but with growth curves for a hypothetical cold-adapted species (dashed line) and warm-adapted species (dotted line) included for reference